Precision Triple-Slot Experiment in the Microwave Regime

A thesis submitted towards partial fulfilment of
BS-MS Dual Degree Programme

by

SHREYA RAY

under the guidance of

URBASI SINHA

Associate Professor, Raman Research Institute,
Bengaluru

Indian Institute of Science Education and Research
Pune

Certificate

This is to certify that this thesis entitled PRECISION TRIPLE-SLOT EXPERIMENT IN THE MICROWAVE REGIME submitted towards the partial fulfilment of the BS-MS dual degree programme at the Indian Institute of Science Education and Research Pune represents original research carried out by SHREYA RAY at RAMAN RESEARCH INSTITUTE, under the supervision of URBASI SINHA during the academic year 2013-2014.

Student
SHREYA RAY

Supervisor
URBASI SINHA

Acknowledgements

First of all, I would like thank my supervisor Dr. Urbasi Sinha for giving me the opportunity to work under her in this project, providing me a great chance to learn so much about my favourite subject. I thank our collaborators, Dr. Ravi Subrahmanyan and Dr. Udaya Shankar, for significant inputs into the project. The next person I want to thank is inevitably Anjali, my colleague and partner in this project. Without her things would have been much trickier and very dull indeed. I thank my other colleagues, Rengaraj, Debadrita, Animesh, Pradeep and Aravind for making the environment lively and for never being reluctant to help me out whenever they could. The brief visit from Prof. Barry Sanders and his student Ish was a very fruitful one and I can never thank them enough for their warmth and for how much I learnt from them. I also thank Reena, Rahul, Shivam and Wasim for useful discussions on various topics. I thank Mahendra for helping me convert my word documents to Latex. The RRI workshop deserves applause for their promptness in arranging for equipment whenever we required them. I thank my roommate Karishma for staying with me through this journey and providing much comfort. Lastly, I must thank everybody in RRI for making my stay such a memorable one.

Abstract

The standard method for calculating the resultant field in a multiple-slit interference experiment, based on solutions for the cases that all but one slit is blocked, yields an incorrect answer. This error leads to incorrect predictions for precise tests of generalised quantum theories. By treating the slit-interference problem as a boundary value problem, we find a better method to deal with slit-interference. We try to verify the results of this theory though experiments in the microwave regime, which being macroscopic, has got many peculiarities. By conducting an experiment that is precise enough to detect a small correction term to the standard theory, we lay the foundation for future experiments to verify a generalised quantum measure theory proposed by Sorkin.

Contents

Chapter 1

Introduction

The Young's Double-Slit experiment has been the most common way of introducing students to quantum mechanics. We have learnt how to interpret the pattern of light and dark fringes on the screen by constructive and destructive interference. On the quantum scale, where wave-particle duality is displayed, and hence Born Rule, Young's Double-Slit experiment is an excellent way to demonstrate the wave nature of "particles". We have always applied the principle of superposition to calculate the interference pattern due to two slits. In our project, we demonstrate that this method of superposition has been incorrectly applied to the Double-Slit interference. We also find the "correction terms" that may be added in order to get the complete picture. This is very useful for two reasons: (1) Attack a wrong theory we have all grown surprisingly so comfortable with, (2) Develop a more accurate and useful theory of slits that may be used in case of precision slit experiments in the future. There is yet another dimension to this problem that primarily arises because we choose to perform the Triple-Slit interference experiment instead of the Double-Slit. A Triple-Slit experiment allows us to test Sorkin's claim of a "third-order interference", which can challenge Born Rule. However, this can only happen if this third-order interference term is big enough to be seen within the precision of our experiment. If Sorkin's claim proves to be true, it can serve as a starting point for further generalisation of quantum mechanics which might lead to a unification of quantum mechanics and general relativity, and get us closer to a Grand Unified Theory.

1.1 Understanding the Problem

In the Double-Slit interference problem, we use the principle of superposition to directly add independent contributions from both slits.

$$\psi_{AB} = \psi_A + \psi_B \tag{1.1}$$

Here ψ_A is the wave function when both slits are open and ψ_A and ψ_B are the wave functions when only one of the slits are open, slit A and slit B respectively. Although superposition principle is valid, it has not been correctly applied in the two-slit case. However, luckily (or unluckily), it has been giving us results consistent with observation. This is because we have never done a Double-Slit experiment that is precise enough.

When we approach the Double-Slit problem by treating ψ_{AB},ψ_A and ψ_B as solutions of differential equations (Maxwell's Equations or Schrodinger's Equation) with different boundary conditions, we find no reason to expect such a simple additive relation between these solutions to different boundary value problems.

One convenient way of analysing these differential equations is by using Feynman's Path Integral formalism, where a wave function can be looked up on as a set of possible paths in space while keeping intact the boundaries. The reason ψ_A and ψ_B don't simply add up to give ψ_{AB} is because in the case of the configuration that gives ψ_{AB} where both slits A and B are open, more paths are possible than the number of paths made possible by adding up the paths due to slit A and the paths due to slit B. These extra paths are the "looped paths", that is, paths that travel through slit A, then through slit B, and again through slit A, therefore traversing a "loop" before hitting the detector. Of course paths may loop around many times. Clearly, such "looped paths" are not possible if one of the slits are closed. We shall represent the contributions due to such paths as ψ_L and include it in the original equation.

$$\psi_{AB} = \psi_A + \psi_B + \psi_{L,2} \tag{1.2}$$

Upon extending this analysis to the triple-slit case, we have the following.

$$\psi_{ABC} = \psi_A + \psi_B + \psi_C + \psi_{L,3} \tag{1.3}$$

Let us momentarily digress to Sorkin's 1994 paper. Sorkin treats quantum measure theory as a special case of a generalised measure theory. He describes a hierarchy of possible sum-rules, each of which implies its successor. The additivity of classical probabilities is only the first in this hierarchy, and the

additivity of quantum amplitudes is the second. If a higher-order sum-rule is valid, we must have the third-order interference term.

$$\begin{aligned} I_3 &= |\,\psi_{ABC}\,|^2 - |\,\psi_{AB}\,|^2 - |\,\psi_{BC}\,|^2 - |\,\psi_{AC}\,|^2 \\ &\quad + |\,\psi_A\,|^2 + |\,\psi_B\,|^2 + |\,\psi_C\,|^2 \neq 0, or \end{aligned} \tag{1.4}$$

$$\begin{aligned} I_3 &= |\,\psi_A + \psi_B + \psi_C\,|^2 - |\,\psi_A + \psi_B\,|^2 - |\,\psi_B + \psi_C\,|^2 - |\,\psi_C + \psi_A\,|^2 \\ &\quad + |\,\psi_A\,|^2 + |\,\psi_B\,|^2 + |\,\psi_C\,|^2 \neq 0 \end{aligned} \tag{1.5}$$

Both classical and quantum measure theories predict the value of I_3 to be zero. This is a necessary condition to be satisfied if the quadratic relationship between quantum amplitudes and probabilities, known as Born Rule, is valid. With the help of a triple-slit experiment we can verify if this third-order interference term is really zero, and therefore this experiment can act as a null-test for Born Rule.

However, Sorkin had overlooked the contribution from looped paths in implying Equation (1.5) from Equation (1.4). Although the contribution from looped paths may be small, it is not negligible. In a precise experiment it will still cause I_3 calculated from Equation (1.4) to be non-zero, and therefore mislead us into believing a violation of Born rule.

1.2 An Experimental Approach to Solve the Problem

We have theoretically determined the contribution from looped paths, $\psi_{L,3}$ to the calculation of I_3.We now seek to experimentally measure I_3, for which we require an extremely precise experiment. We have gradually tried to improve the precision of our experiment.
The contribution from looped paths, $\psi_{L,3}$ to the calculation of I_3 can be conveniently represented by a dimensionless number κ, defined as:

$$\kappa \equiv \frac{I_3}{I_2} \tag{1.6}$$

where I_2 is a sum of the second order interference term for various pairs of slit combinations from the three slits A, B and C.

$$I_2 = I_{2,AB} + I_{2,BC} + I_{2,CA} \tag{1.7}$$

In *Sinha et al., 2010*, an upper bound to the value of κ was found to be of the order of 10^{-2}. The exact value of κ could not be found due to limitation in the precision of the experiment, which was performed at 810nm. Unless our experimental accuracy is improved beyond this limit, it is not possible to use the triple-slit experiment for testing Born Rule.

A unique feature of our current experimental approach is that we are performing these experiments in the microwave regime, in parallel to the one being performed in the optics lab at 810nm. Since we are performing traditionally optics experiments using microwaves, which involve drastically different length scales, we have been required to address new problems at every step and our experimental design has been continuously evolving. The advantage of using microwaves is that, the set-up being macroscopic, we can manipulate many details which would otherwise be very difficult in the optics experiment, like continuously changing the inter-slit distance which has a significant impact on κ as we shall see. In fact, we can choose the inter-slit distance that gives a larger value for κ.

1.3 A Brief History of the Problem

For many years now, Quantum Mechanics and General Relativity haven't really been the best of friends, which is to say, the range of phenomena explained by these two competent theories hardly have any overlap. Physicists continue to look for a Grand Unified Theory that might be able to explain every kind of phenomenon in the Universe. In the quest to find a Grand Unified Theory, attempts have been made to generalise both these theories and expand the domain of phenomena they can explain.

Ever since its conception, Quantum Mechanics has successfully dealt with many a blow that has come its way. Never mind much of its subtlety and counter-intuitiveness, Quantum Mechanics has stood the test of time and has been repeatedly verified by experiments. However, there remain mysteries and paradoxes associated with this theory which hint at the possibility of the existence of perhaps a more generalised version of the theory.

In his 1994 paper, Sorkin attempted to generalise the quantum measure theory to a generalised measure theory that would have the quantum measure theory as a limiting case, and in the process proposed a null-test for Born Rule using a simple triple-slit experiment.

Raymond Laflamme's group at the Institute for Quantum Computing, Waterloo, in collaboration with Gregor Weihs and Sorkin, performed a triple-slit experiment on these lines but could not measure a non-zero κ within the precision range of the experiment, thus leaving Born Rule valid within the

limit of the precision. The results were published by *Sinha et al.* in the year 2010. In 2011, *Hans de Raedt et al.* performed very high-accuracy simulations to show that if the slit interference is treated as a boundary value problem then κ would invariably be non-zero even without any higher-order interference. The programs were based on Maxwell's equations and used a Finite Difference Time Domain (FDTD) method to propagate.

Therefore, if we are to carry out the triple-slit test for Born Rule as suggested by Sorkin, we have to first take care of the effect of boundary conditions. One efficient way to do this is by invoking the concept of "looped paths" and characterising the contribution from these paths to the triple-slit interference pattern. In a recently submitted paper, our lab has treated the slit interference problem in the Feynman's Path Integral Formalism to derive κ in a much easier way, by also weighing the looped paths along with the direct paths. We explore many other theoretical approaches to calculate κ. Attempts to experimentally demonstrate the contribution of looped paths are ongoing.

Chapter 2

Theory

Understanding and realisation of this experiment required knowledge spread out in three different disciplines: diffraction of waves, quantum mechanics and radiofrequency electronics. This chapter recapitulates the various concepts in these fields that are directly related to the experiment. We also give a detailed description of the theory of 'looped paths' and any other theories that we have developed in the course of the experiment.

2.1 Diffraction Theory

Our experiment concerns itself with diffraction of electromagnetic waves, therefore certain theories have played a very important role in shaping our experimental design.

2.1.1 Huygens Principle and the Eikonal Approximation

Huygens principle is a method of analysis of problems relating to wave propagation. According to Huygens principle, every point on a wave-front can be considered as a source of secondary spherical wavelets. The next wave-front is formed from superposition of these wavelets. Once again, the points on this new wave-front can be treated as sources of secondary wavelets and so on. In this manner, the form of the wave can be determined at any time during its propagation. Huygens principle is applicable to both near field as well as far field limits.

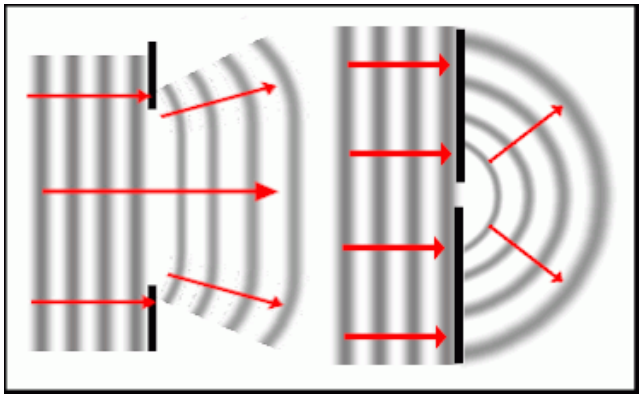

Figure 2.1: In the Eikonal approximation, travelling wavefronts are approximated by straight lines.

Huygens principle is often expressed in its Eikonal approximation, or the straight line approximation. The picture of wave propagation is replaced by one of travelling straight line paths. This is similar to the WKB approximation in that it reduces the equations to a differential equation in a single variable. This single variable is described by the trajectory of the particle. (In Feynman's Path Integral formalism, this variable is the classical action of a path).

Consider a point P on any wave-front, having complex amplitude A. Consider another point Q at a distance x away. If k is the wave number associated with the wave in consideration, the complex amplitude of the wave arriving at Q from point P is given as

$$A(Q)_P = \frac{A(P) \times e^{ikx}}{x} \tag{2.1}$$

In order to find the total complex amplitude at Q, one needs to sum (or integrate) over all such contributions from the other points on the wave-front containing P.

$$A(Q) = \sum_P \frac{A(P) \times e^{ikx}}{x} \tag{2.2}$$

The theoretical predictions of interference patterns in most of our experiments have been made using a code that is based on this principle.

2.1.2 Near Field and Far Field

Regions of electromagnetic field around a radiating object can be classified into two regimes: the near field and the far field. The near field can be further

divided into a reactive on non-radiative near field and a radiative near field. The radiative near field in also known as the Fresnel region and the far field is also known as the Fraunhofer region.

The reactive near field is located in the immediate vicinity of the radiating object and is not of much interest to us. Here the electric and magnetic fields are out of phase with each other and their magnitudes may be different from each other. These fields interact with the object via electromagnetic induction and therefore affect its radiation pattern.

The fields somewhat stabilise and radiating fields begin to emerge upon entering the Fresnel region. The fields die off as $\frac{1}{R}$ and the power density dies off as $\frac{1}{R^2}$. The shape of the radiation pattern still varies appreciably with distance. Consider a radiating object of dimension D and the wavelength of radiation being λ. If the distance from this object is given as R then the Fresnel region is defined by

$$0.62\sqrt{\frac{D^3}{\lambda}} < R < \frac{2D^2}{\lambda} \tag{2.3}$$

Beyond this region is the far field or the Fraunhofer region. Here, the radiation pattern does not change shape with distance. The electric and magnetic fields are orthogonal to each other and to the direction of propagation, as with plane waves.

Although the above formula (2.3) gives a quantitative definition, in terms of behaviour of radiation the boundary between these regions is not very precisely defined. A quantity called Fresnel number (F) often gives a qualitative idea of how near field or how far field we are.

$$F = \frac{D^2}{R\lambda} \tag{2.4}$$

To be in the far field we must have $F << 1$. The exact value of F required to be in the far field depends on the shape and configuration of the source. $F < 0.01$ is usually a reasonable approximation.

In the phenomenon of diffraction, electromagnetic waves are scattered by an obstruction. Even in this case, the same definitions of Fresnel and Fraunhofer regions are valid. Diffraction produces an interference pattern which may be studied close to the diffracting object (Fresnel diffraction) or far away from it where the pattern does not change any more with distance (Fraunhofer diffraction). We have performed experiments in both Fresnel and Fraunhofer regions, although our target is to try and remain in the Fraunhofer region which is mathematically simpler.

2.1.3 Babinet's Principle and Introduction to Slots

Babinet's principle states that the field at any point behind a plane having a screen, if added to the field at the same point with the complementary screen, gives us a field that is equal to the field at that point when no screen is present. Two diffracting screens are said to be complementary when the transparent regions of one correspond to the opaque regions of another and vice-versa.

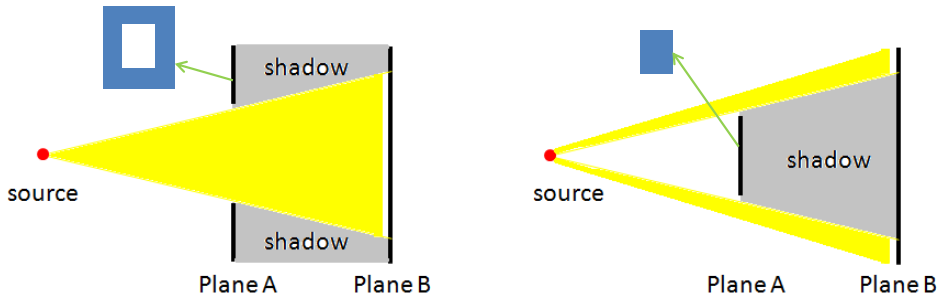

Figure 2.2: Pattern detected at plane B in two cases having complementary screens at plane A.

In the above figure 2.2, consider a perfectly absorbing metal plate placed at plane A. Then at plane B of the screen there is a region of shadow. Let the field at plane B be some function $f_1(x, y, z)$. Replace the screen S by its complementary screen such that the metal portion is replaced by free space and vice-versa. Let the field at plane B now be some function $f_2(x, y, z)$. When no screen is present at plane A, let the field at plane B be given by some function $f_0(x, y, z)$.
Then, from Babinet's principle,

$$f_1(x, y, z) + f_2(x, y, z) = f_0(x, y, z) \tag{2.5}$$

If we go sufficiently far away from the source, intensity falls of as $\frac{1}{R^2}$ and almost tends to zero. In that case,

$$f_0(x, y, z) \sim 0$$

$$\begin{aligned} \Rightarrow f_1(x, y, z) + f_2(x, y, z) &= 0 \\ \Rightarrow f_1(x, y, z) &= -f_2(x, y, z) \\ \Rightarrow \mid f_1(x, y, z) \mid^2 &= \mid f_2(x, y, z) \mid^2 \end{aligned} \tag{2.6}$$

Since intensity is given by square of the field, the diffraction pattern due to complementary screens are identical (except for the overall forward beam intensity) when viewed from a distance sufficiently far away from the screen.

Babinet's principle holds for a very wide range of cases. The source may be a point source as in the example, or some distribution of sources. The principle also applies when the surface of the screen does not necessarily lie on a single plane as in our example.

This inspired us to use slots, or plates, instead of slits in our experiment. 'Slots', as we call them, are complementary screens to slits. Initially, we had wanted to perform a slit-interference experiment. However, in the microwave regime of around 6GHz, our experimental dimensions were so large that the slits required would be large but the opaque screen into which the slits should be cut had to be of enormous and unpractical size. The screen had to be so large so that we could minimise the diffraction from its edges by letting the intensity fall significantly at these edges, otherwise the diffraction pattern of the edges of the screen would dominate and drown the slit-interference pattern, as we could see from our simulations.

2.2 Quantum Mechanics and Quantum Measure Theory

An important purpose of our experiment is to improve the theory of slit interference and increase the precision of the experimental design, so that we are in a position to test Sorkin's claim about the existence of higher order interference. As stated in detail in Sec. 1.1, the current theoretical framework in use for treating interference due to slits is not accurate and requires correction if we are to go ahead and perform a triple-slit interference experiment that could serve as a null-test for Born Rule. A recap of the following theories will help appreciate the bigger picture.

2.2.1 Feynman's Path Integral Formalism and the 'Looped Paths'

Feynman's Path Integral formalism today is rarely used in the study of formal Quantum Mechanics, the focus instead being on the Schrodinger formalism. The concept of path integral, however, is widely used in the study of Quantum Field Theory. We tried to predict the correction term κ to the triple-slit interference using this formalism.

Conventionally, when we solve a problem in Quantum Mechanics, we first

try to find out the time evolution operator ($U(t) = e^{-iHt}$), by finding out the Hamiltonian of the system. However, in the path integral approach we directly find $U(t)$. In order to find $U(t)$ we use the following algorithm:

- Draw all paths connecting the initial position (x, t) and the final position (x', t') in the x-t plane.
- Find the classical action $S[x(t)]$ for all these paths.
- $U(x, t; x', t') = A \sum_{allpaths} e^{\frac{S[x(t)]}{\hbar}}$

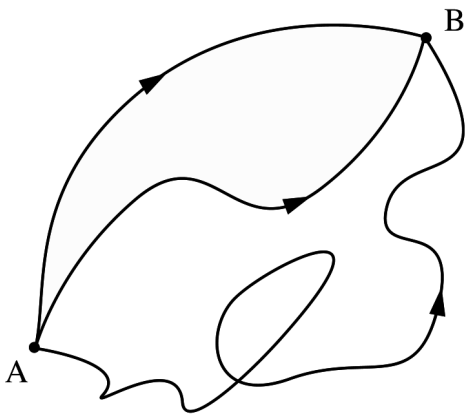

Figure 2.3: In going from A to B, contribution from all the possible paths are summed over.

In the above summation, every path including the classical trajectory contributes to the summation with the same amplitude. However, since every path has a different classical action $S[x(t)]$ the paths contribute to the summation with different phases. This causes the contribution from most paths to get cancelled out until we get closer to the classical trajectory. $S[x(t)]$ is stationary near the classical path and there is constructive interference here. As we move away from the classical trajectory, destructive interference sets in. Therefore, although the classical path may not contribute a lot to the summation by itself, the coherent contribution from its vicinity paths make the classical trajectory very important.

We are, however, dealing with the non-classical looped paths in our experiment. These looped paths are a direct manifestation of the difference in

boundary conditions: they are the reason why in a double-slit experiment we cannot add the two cases where only one of the slits is open, to get the result of the case when both slits are open. These looped paths cannot exist when one slit is open but comes into the picture only when both slits are open.

In our triple-slit experiment, we calculated the contribution from looped paths in the following manner:

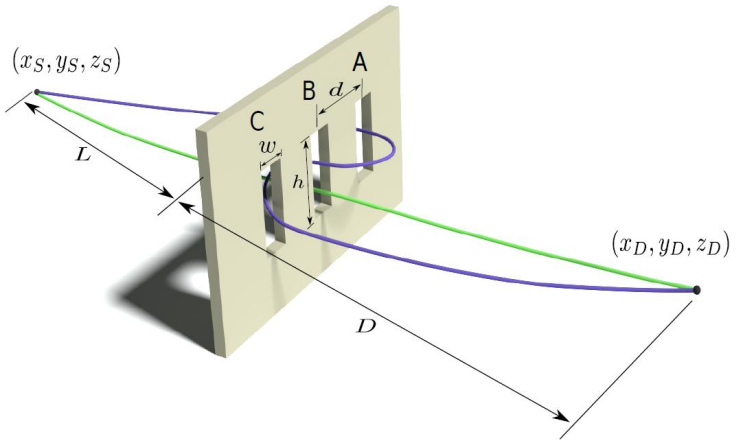

Figure 2.4: Illustration of a classical path (green) and a non-classical looped path (purple) in the triple-slit case.

1. All the classical paths include:

$$U_0 = \left[\left(\sum_S^A e^{\frac{S[x(t)]}{\hbar}}\right) \times \left(\sum_A^D e^{\frac{S[x(t)]}{\hbar}}\right)\right] + \left[\left(\sum_S^B e^{\frac{S[x(t)]}{\hbar}}\right) \times \left(\sum_B^D e^{\frac{S[x(t)]}{\hbar}}\right)\right] \tag{2.7}$$

2. First-order looped paths include terms like:

$$U_{1,AC} = \left[\left(\sum_S^A e^{\frac{S[x(t)]}{\hbar}}\right) \times \left(\sum_A^P e^{\frac{S[x(t)]}{\hbar}}\right) \times \left(\sum_P^C e^{\frac{S[x(t)]}{\hbar}}\right) \times \left(\sum_C^D e^{\frac{S[x(t)]}{\hbar}}\right)\right] \tag{2.8}$$

Where P is an arbitrary point on any of the slits, and the sum is taken over P to account for all the possible looped paths that traverse the slits A and C. We have similar terms for looped paths that traverse the slits A and B or the slits B and C.

3. In the same manner we can analyse higher-order loops that cross the slit-plane multiple number of times. However, their contribution is negligible.

2.2.2 The Quest for a generalised Quantum Measure Theory

In his 1994 paper, Rafael Sorkin proposed a generalised measure theory which includes quantum mechanics as a special case. He described a hierarchy of possible sum-rules, each of which implies its successor. The additivity of classical probabilities is only the first in this hierarchy, and the additivity of quantum amplitudes is the second.
For two disjoint events, classical probability gives

$$Probability(A+B) = Probability(A) + Probability(B)$$

$$\rightarrow I_2 \equiv Probability(A+B) - Probability(A) - Probability(B) = 0 \quad (2.9)$$

where I_2 has been defined as a second-order interference term.

However, for two disjoint events, quantum measure theory gives

$$\mid \psi_{AB} \mid^2 = \mid \psi_A + \psi_B \mid^2 = \mid \psi_A \mid^2 + \mid \psi_B \mid^2 + \psi_A^* \psi_B + \psi_B^* \psi_A \quad (2.10)$$

$$\rightarrow I_2 = \mid \psi_A + \psi_B \mid^2 - \mid \psi_A \mid^2 - \mid \psi_B \mid^2 = \psi_A^* \psi_B + \psi_B^* \psi_A \neq 0 \quad (2.11)$$

So the second order interference term is non-zero in case of quantum mechanics, which directly violates the laws of classical probability. The probabilities don't add but the mysterious complex amplitudes governing them do. The behaviour of quantum probabilities is governed by Born Rule and the quantum measure theory, but its interpretation remains an open question.

Let us move one step ahead in the hierarchy and consider three disjoint events. Once again classical probability theory gives:

$$\begin{aligned}
Probability(A+B+C) &= Probability(A) + Probability(B) + Probability(C) \\
Probability(A+B) &= Probability(A) + Probability(B) \\
Probability(B+C) &= Probability(B) + Probability(C) \\
Probability(C+A) &= Probability(C) + Probability(A)
\end{aligned}$$

$I_3 \equiv Probability(A+B+C) - Probability(A+B) - Probability(B+C) - Probability(C+A) + Probability(A) + Probability(B) + Probability(C) = 0$

Now for three disjoint events, quantum measure theory gives:

$$\begin{aligned}
|\psi_{ABC}|^2 &= |\psi_A+\psi_B+\psi_C|^2 \\
|\psi_{ABC}|^2 &= |\psi_A|^2+|\psi_B|^2+|\psi_C|^2+\psi_A^*\psi_B+\psi_B^*\psi_A \\
&\quad +\psi_B^*\psi_C+\psi_C^*\psi_B+\psi_C^*\psi_A+\psi_A^*\psi_C \qquad (2.12)\\
|\psi_{AB}|^2 &= |\psi_A+\psi_B|^2=|\psi_A|^2+|\psi_B|^2+\psi_A^*\psi_B+\psi_B^*\psi_A \\
|\psi_{BC}|^2 &= |\psi_B+\psi_C|^2=|\psi_B|^2+|\psi_C|^2+\psi_B^*\psi_C+\psi_C^*\psi_B \\
|\psi_{CA}|^2 &= |\psi_C+\psi_A|^2=|\psi_C|^2+|\psi_A|^2+\psi_C^*\psi_A+\psi_A^*\psi_C
\end{aligned}$$

$$\rightarrow I_3=|\psi_{ABC}|^2-|\psi_{AB}|^2-|\psi_{BC}|^2-|\psi_{CA}|^2+|\psi_A|^2+|\psi_B|^2+|\psi_C|^2=0 \qquad (2.13)$$

So we observe that the third order interference is zero in the case of both classical and quantum measure theory. In this sense, quantum randomness preserves something of the classical additivity of probabilities.

Instead of regarding quantum mechanics as a modified form of probability theory, we can interpret it as the limit of a generalised measure theory, which might govern many other events in the universe. It is also possible that we might find a violation of the quantum measure theory within quantum mechanics itself, if I_3 is found to be non-zero in experiments, therefore violating Born rule. In that case, some sort of tri-linear form associated to I_3 would presumably replace the familiar inner product of quantum Hilbert space. Beyond I_3, in the presence of even higher order interference terms, one would expect a kind of multi-linearity. Sorkin associates this kind of multi-linearity to a developing, incomplete 'future' which grows at its tips like a tree.

2.3 Radiofrequency Electronics

This section contains a brief description of a few topics dealing with electronics and instrumentation in the radiofrequency regime that will be helpful in understanding our experimental set up and the results of our experiment.

2.3.1 The Half-Wave Dipole Antenna

The dipole antenna is an open-circuited wire, fed at its centre. How efficiently a dipole antenna radiates depends on its length relative to the wavelength of the alternating signal being fed to it. The half-wave dipole antenna, with length equal to the half of the wavelength at the frequency of operation has the highest efficiency. At any smaller length, the peak value of current is not reached along the dipole.

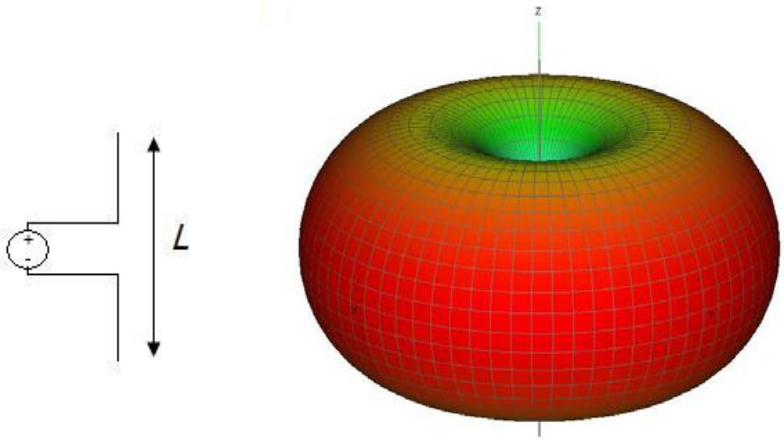

Figure 2.5: A dipole antenna (left) and its 3D antenna radiation pattern in the far field (right).

In all of our experiments we have used dipole antennas for transmitting microwaves at around 6GHz, since they were the most readily available antennas. The radiation pattern of an antenna shows how the power radiated by an antenna varies as a function of direction at some point in the far field of the antenna. The radiation pattern of a dipole antenna looks rather like a donut. It has got two kinds of curvature, or two radii. Since we wanted the radiation intensity to be as uniform over the slots as possible, we made sure that our arrangement of slots always faced the larger radius of this donut and hence the less curved surface.

The dipole antenna is highly symmetric about the vertical axis (wire axis). Since it radiates uniformly in all directions in a given horizontal plane, we say it has a low directivity. The advantage of low directivity is that it is usually accompanied by high radiation efficiency but the drawback is that the radiated power falls rapidly along any direction.

2.3.2 Important Antenna Parameters

2.3.2.1 VSWR

VSWR stands for Voltage Standing Wave Ratio, and is also referred to as Standing Wave Ratio (SWR). The parameter VSWR numerically describes how well the antenna is impedance matched to the transmission line it is connected to.

To deliver power to an antenna, the impedance of the transmission line must be well matched to the antenna's impedance. When an antenna is not matched to the receiver, power is reflected (so that the reflection coefficient $\Gamma \neq 0$).This causes a "reflected voltage wave", which creates standing waves along the transmission line. Therefore, VSWR is a function of the reflection coefficient, which describes the power reflected from the antenna.

$$VSWR = \frac{1+ \mid \Gamma \mid}{1- \mid \Gamma \mid} \tag{2.14}$$

Physically, VSWR is the ratio of the peak amplitude of a standing wave to the minimum amplitude of a standing wave, determined from the voltage measured along a transmission line leading to an antenna.

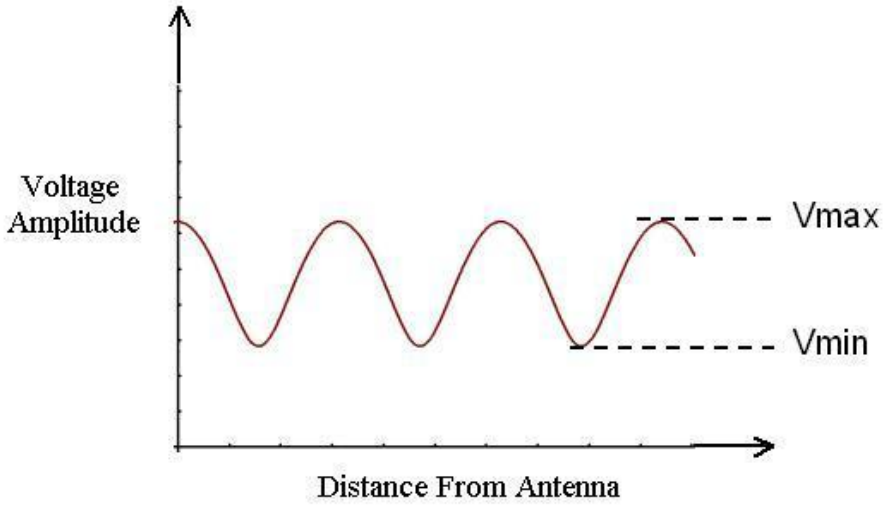

Figure 2.6: Standing voltage wave in the transmission line caused due to non-zeroness of reflection coefficient.

Being a ratio, VSWR is always real and positive. The smaller the VSWR is, the better the antenna is matched to the transmission line and the more power is delivered to the antenna. The minimum VSWR is 1.0. In this case, no power is reflected from the antenna and the voltage has a constant magnitude along the transmission line, which is ideal.

2.3.2.2 Bandwidth

The bandwidth of an antenna is defined as the range of frequencies within which the performance of the antenna conforms to a specified standard. In

practice, it is usually the range of frequencies for which the antenna has a comparatively low VSWR.

2.3.2.3 Antenna Q

The Q of an antenna is a measure of the bandwidth of an antenna relative to the centre frequency of the bandwidth. If the antenna operates over a band between f_1 and f_2 with centre frequency $fc = \frac{(f1+f2)}{2}$, then the Q is given by:

$$Q = \frac{f_C}{f_2 - f_1}$$

Antennas with a high Q are narrow band and antennas with a low Q are wideband. The higher the value of Q, the more sensitive the input impedance is to small changes in frequency. We seek to design an antenna with a high Q to make our experiment more precise.

2.3.3 The Quarter-Wave Choke Sleeve Antenna

The quarter-wavelength choke-sleeve antenna is a coaxial antenna that is a more convenient alternative to the half-wave dipole antenna. Radiation patterns of the two are practically very similar and therefore these QWCS antennas are suitable for use in experiments that conventionally use half-wave dipole antenna. QWCS antennas are easy to construct, naturally adapted to coaxial input connection therefore avoiding the use of a balun, and also avoid the problematic T-shaped structure that occurs in case of a dipole antenna. Moreover, being of a compact shape with an adjustable sleeve radius, they can be inserted even into small spaces.

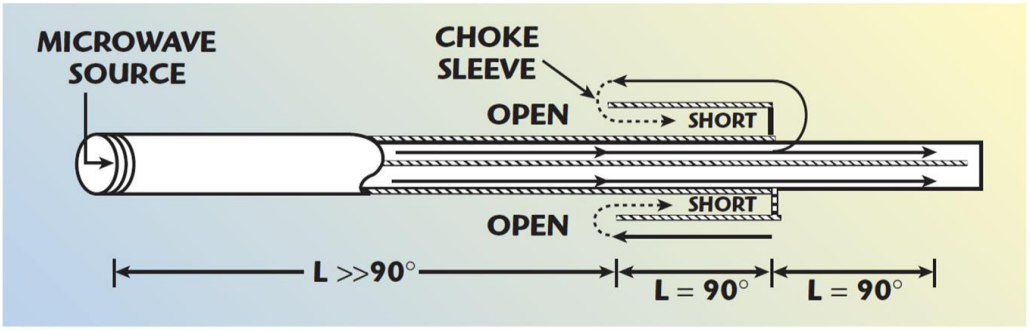

Figure 2.7: Parts of a quarter-wave choke-sleeve antenna.

From the end of the coaxial wire, part of the wave radiates outward from the exposed inner conductor, and another part radiates from the quarter-wavelength choke-sleeve section that presents an open circuit at the end (after bending over). Due to this shorted end of the choke sleeve presenting an open circuit to a microwave signal that would otherwise travel back along the choke sleeve toward the source, there is a tendency to confine the radiating source to the half-wavelength region between the open end of the choke sleeve and the exposed inner conductor of the coaxial line. The choke sleeve also prevents wave propagation back along the outer conductor. A larger radius of choke sleeve approximates the case of half-wave dipole antenna even more closely.

2.3.4 Free Space Loss (FSPL)

Free space Loss is the loss in signal strength of an electromagnetic wave travelling in free space, without any obstacles to cause reflection or refraction. FSPL is independent of hardware imperfections. If d is the distance between transmitter and receiver and λ is the wavelength of the wave being transmitted,

$$FSPL = \left(\frac{4\pi d}{\lambda}\right)^2 \tag{2.15}$$

A knowledge of the FSPL is necessary for determining the distance range up to which we can perform our experiments.

Chapter 3

Simulations

The triple-slit experiment performed by *Sinha et al., 2013*, was done at a wavelength of 810nm. In our current experiment we are, however, dealing with a totally different realm, a wavelength of the order of centimetres, which makes it a macroscopic realm. Therefore we can't simply extend the experimental design of the optics experiment at 810nm into this realm, and we have to start from scratch.

Antennas seemed to be an amenable source of microwaves for our experiment, especially because we could harness the expertise in antennas by collaborating with the radio-astronomy department at RRI. In order to perform the experiment, we had to first simulate it so that we could have a fair idea of the parameters to start with - the wavelengths, distances and slot dimensions. For our initial simulations we used WIPL-D, which is an EM-solver software popular among experimenters in microwaves. We ran various simulations in order to understand the best parameters for observing a kappa of significant size. Later on, we also used codes written in Mathematica, MATLAB, python and C. The following is a chronology of our various approaches towards simulation in order to arrive at the best achievable experiment design.

3.1 Initial Simulation Techniques

These are the simulations we began with much before setting up the actual experiment, in order to decide up on the experimental parameters to begin with and have certain expectations from the experimental outcomes.

3.1.1 Feynman's Path-Integral Formalism in Mathematica: 5GHz

When we started the experiment, the most readily available sources of microwaves to us were the signal generators of the radio-astronomy department. One went up to 3GHz and another went up to 6GHz. We decided to simulate how our experimental results would look if we worked with these frequencies. The programme was written by my colleague and had a simple algorithm based on Feynman's path-integral formalism. It assumed plane-wave propagation from source and integration was performed directly over all possible paths: the non-bending paths as well as the looped, bending paths (*Rahul Sawant et al., 2013, Whirling Waves in Interference Experiments*). This approach is directly based on the theory of 'looped paths' that our group has developed. At 5GHz ($\lambda = 6$ cm), in the far-field (slot-to-detector distance 3000 cm, Fresnel number = 0.008), and with the parameters slot-width 12 cm, slot-to-slot distance (centre-to-centre) 30cm, slot length 100 cm, antenna-to-slot distance 100 cm, we get the following triple-slot interference pattern using our Mathematica code:

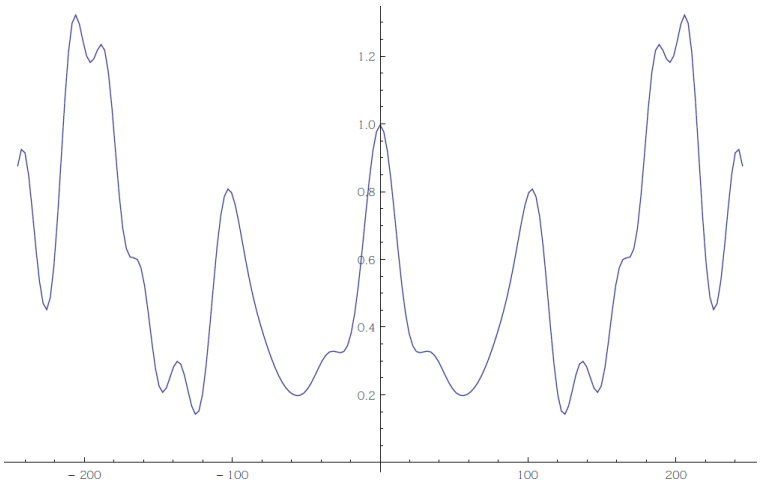

Figure 3.1: Triple-slot interference pattern in Mathematica, using Feynman's Path Integral formalism. X-axis represents position along the line of detection and Y-axis represents intensities in arbitrary units.

The corresponding κ graph looks like the following. Observe that we get a value for κ of the order 10^{-3}.

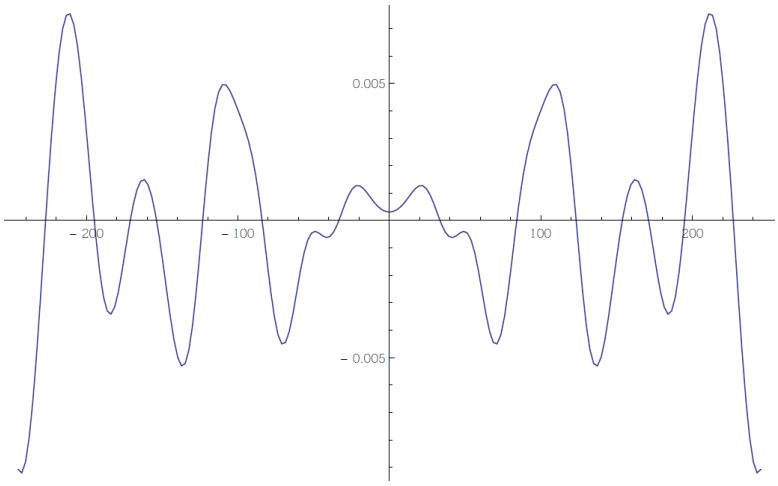

Figure 3.2: κ variation pattern in Mathematica, using Feynman's Path Integral formalism. X-axis represents position along the line of detection and Y-axis represents intensities in arbitrary units.

3.1.2 WIPL-D Electromagnetic Simulations: 5GHz

The simulation described in subsection (3.1.1) is completely based on our theory, and hence on all its implicit assumptions. We wanted to cross-check the results with other simulations. We had assumed that the electromagnetic waves had perfectly planar wave fronts coming from a source at infinity; hence the intensity and phase were uniform over an entire slot. However, for achieving a practical realisation of the experiment, we have to drop these assumptions.

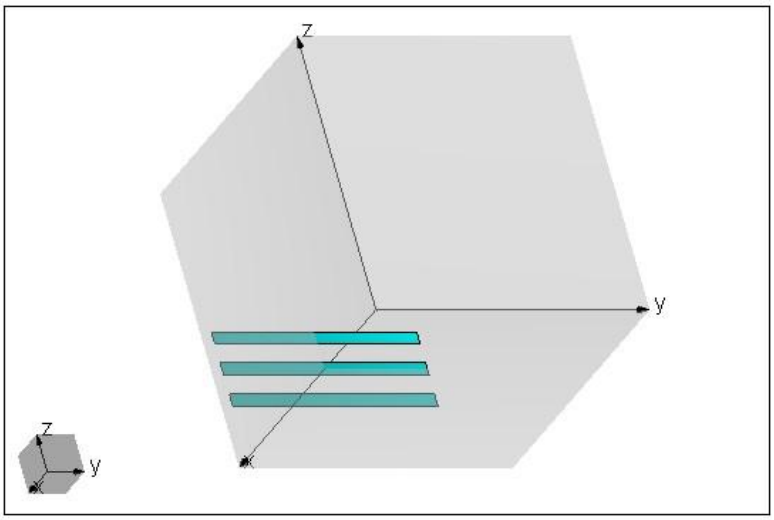

Figure 3.3: Construction of a triple-slot experiment simulation in WIPL-D

WIPL-D is a popular software for microwave simulations, where one can design electromagnetic sources, and their surroundings, and then look at the resulting radiation pattern. We made a model of our experiment in WIPL-D, where the source was a half-wave dipole antenna and the slots were perfectly blocking. We used the same parameters as the Mathematica simulation and results of the simulation were calculated in the far field limit.

Following is the triple-slot interference pattern in the far-field:

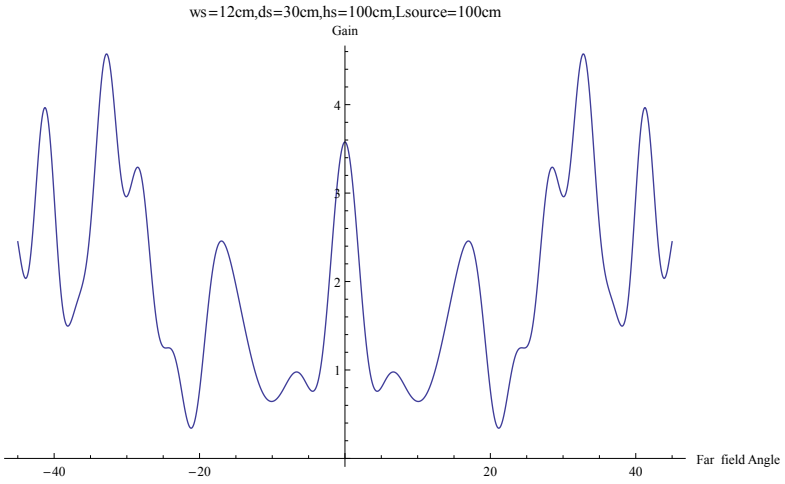

Figure 3.4: Triple-slot interference pattern in the far field using WIPL-D

Following is the graph for corresponding κ variation:

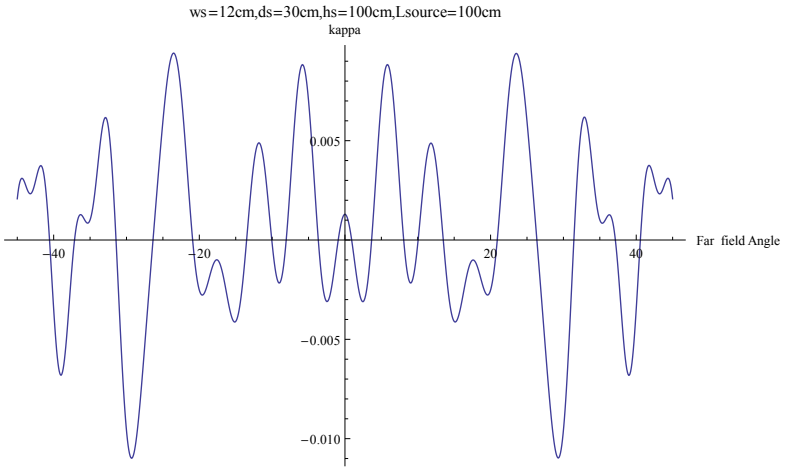

Figure 3.5: κ variation pattern in the far field using WIPL-D

As we can see, the order of magnitude of κ is very similar to the one achieved from the Mathematica programme. However, there is a visible difference in the κ variation along the line of detection. This can be attributed to the plane-wave assumption in the case of the Mathematica simulation, which is absent in the WIPL-D simulation.

Notice that we have simulated for 'slots' and not 'slits'. It was this simulation that made us first realise that using the traditional 'slits' for interference would be impractical for our current experiment, because the screen on which the slits had to be cut out had to be of impractically enormous dimensions in order to escape diffraction effects from the edges of the screen from drowning out the interference pattern we wanted to observe. That lead us to the wonderful alternative of 'slots', the slit and the slot being related to each other through Babinet's Principle (see Sec. 2.1.3).

3.1.3 Markov Chain Monte Carlo Simulations in Mathematica

In order to confirm our theory gives the expected results and to increase our confidence we decided to cross-check our results with those of various other algorithms. A student prior to me had written programmes using Markov Chain Monte Carlo (MCMC) simulations. MCMC methods are widely used for generating random samples for any arbitrary distribution. In this case, a large number of random walks were generated, which includes both direct paths as well as looped paths, to calculate the probability amplitude of each walk which is contributing to the interference pattern. However, the computational costs of these programmes were too high to be able to utilise any of

them on a regular basis.

3.2 Some Conclusions from the Simulations

From the simulations, we concluded certain important things about the experimental design. We also realised some of the possible problems we could face during our experiment and some features which we could exploit, like the inter-slot distance.

3.2.1 The problem of Far Field

There remained an unresolved problem. All our algorithms, as well as the definition of κ, are based on the assumption that we are making our measurements related to the interference pattern detection in the far-field, and hence all the typical far-field assumptions of the Fraunhofer regime are valid (see Sec. 2.1.2).

The far-field of our experiment, however, is very much far away because Fresnel number is directly proportional to the square of the slot-dimension, and the slot-dimension has to be at least twice the size of the wavelength in order to diffract the wave. At 5GHz, the wavelength is 6cm, hence the slot-size has to be at least 12cm. With these parameters, to make the Fresnel number as small as 0.008 (which we used in the optics triple-slit experiment at 810nm), we require the slot-to-detector distance to be around 3000cm, or 30m! This is a distance too enormous for the set-up of a precision experiment.

There seems to be two alternative ways of dealing with this problem. We can either modify our theory and the definition of κ so that the experiment can be performed in the near-field, or we can make use of higher frequency microwaves for our experiment so that the far-field can be pushed closer because of smaller dimensions of slots. We first decided to do the latter. In fact, we wanted to scale down to a frequency of 15GHz, where the wavelength is 2cm, hence the Fresnel number given a slot-size of 4cm is 0.008 at 10m. Suppose we aim for a larger Fresnel number, say twice, that is 0.016, at the cost of sacrificing some precision, the slot-to-detector distance need to be only 5m. 5m is a convenient size, especially because now the experiment can be performed inside a typical anechoic chamber, hence shielded by outside interference and reflections. Therefore, we redid the Mathematica and WIPL-D simulations at 15GHz.

3.2.2 Effect of inter-slot distance on κ

During our initial simulations we also observed that the value of κ increases significantly up on reducing the inter-slit distance. We could use this to our advantage to observe a value for κ that is much greater than the one we were looking for in the 810nm experiment. From the following graphs, one can see how κ increases upon decreasing the slot-to-slot distance.

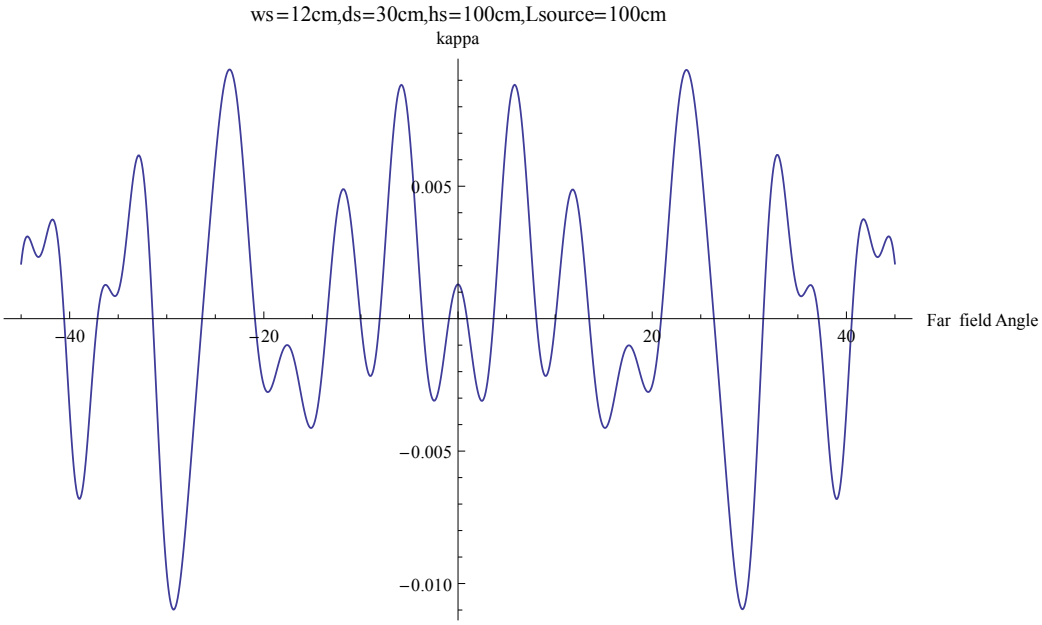

Figure 3.6: κ variation pattern in Mathematica, using Feynman's Path Integral formalism. Interslot distance=30cm

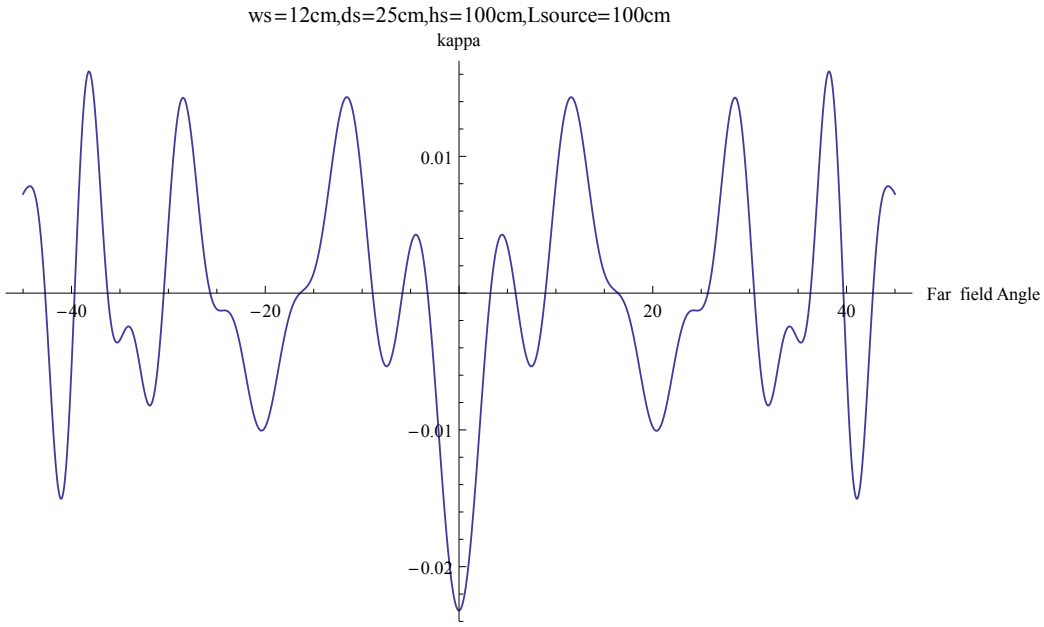

Figure 3.7: κ variation pattern in Mathematica, using Feynman's Path Integral formalism. Interslot distance=25cm

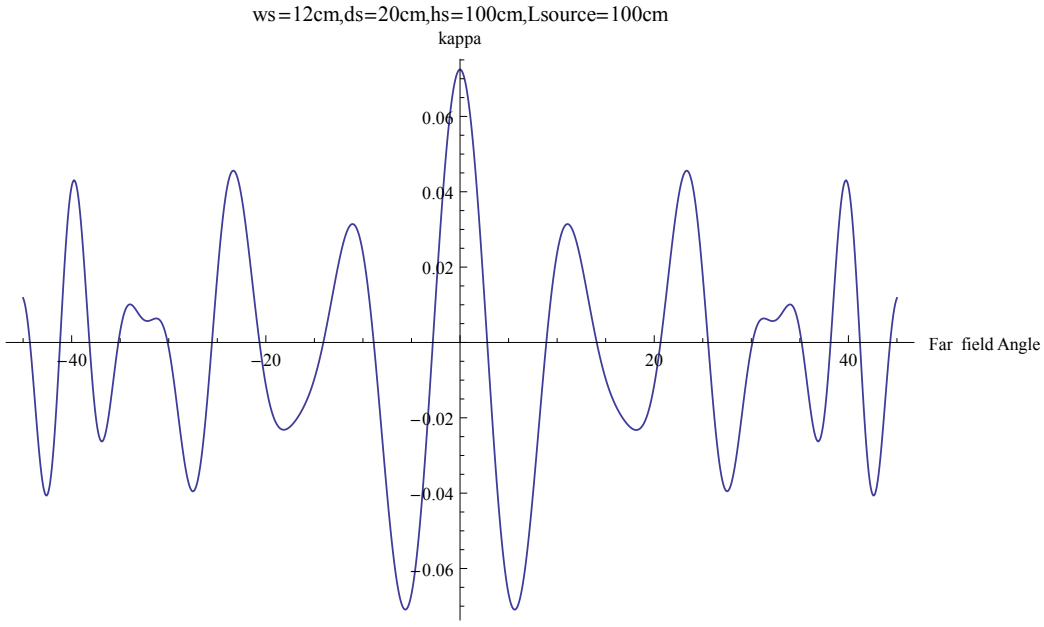

Figure 3.8: κ variation pattern in Mathematica, using Feynman's Path Integral formalism. Interslot distance=20cm

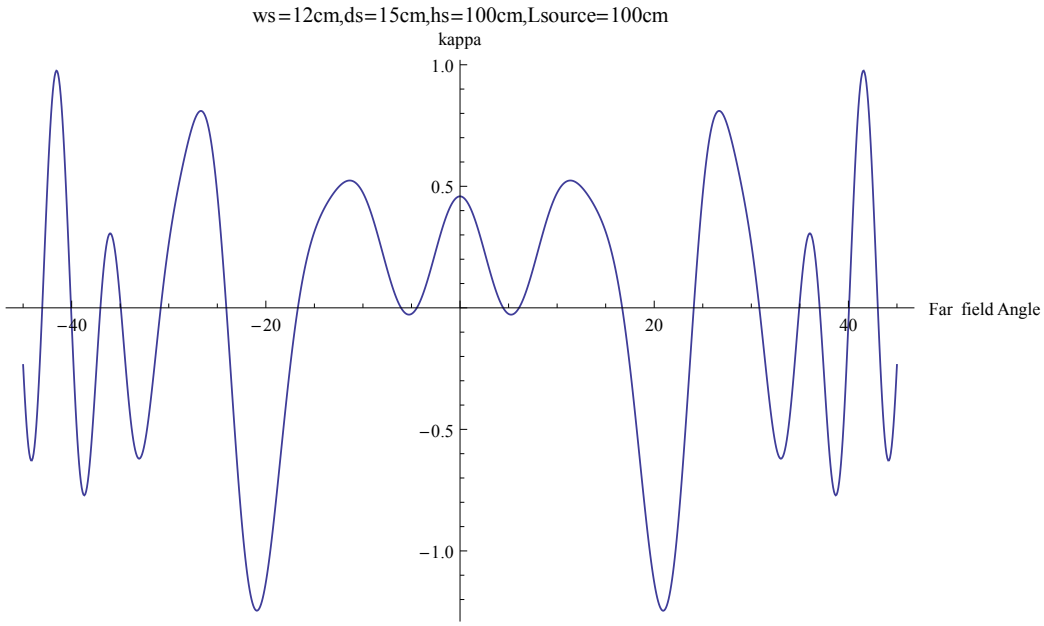

Figure 3.9: κ variation pattern in Mathematica, using Feynman's Path Integral formalism. Interslot distance=15cm

3.3 Simulations for the Experiment

As we started performing the slot-interference experiments, for the purpose of fast analysis we required programmes that would calculate the interference pattern as fast as possible, so that we could assess our data after an experiment and then, in case the results are not satisfactory, immediately modify the experiment and try again. Following are few of the algorithms and programmes we used during our experimental phase.

3.3.1 The Sinc Function formula: 15GHz

There is yet another approach to predict the triple-slit interference pattern: using the Sinc Function formula for n-slit interference. The formula is derived from Fourier transform of an n-slit diffraction grating and is valid within the Fraunhofer diffraction regime for which $R >> a$ and $R >> d$. The source is assumed to be a far-away point source and the detection is done at far-field as well. The intensity at any point with angular position x along the line of detection, when the detection is being done at far-field, is given by the

following formula.

$$I(x) \propto \frac{s}{\lambda R^2}\{\frac{sin(\frac{N\kappa dx}{2})}{sin(\frac{\kappa dx}{2})} \times sinc(\frac{\kappa sx}{2})\}^2 \tag{3.1}$$

where, s = slit width, λ=wavelength, R= distance between slit and detector, N= number of slits, κ=wave number, d=distance between two consecutive slits and sinc(y) $\equiv \frac{sin(y)}{y}$.

At 15GHz (λ=2cm), with the parameters slit-width=4cm, inter-slit distance=12cm, the triple-slit plot is as follows. At sufficiently large distance of detection, the triple-slit pattern should match the triple-slot pattern because of Babinet's Principle (see Sec. 2.1.3). Following is the triple-slit interference pattern.

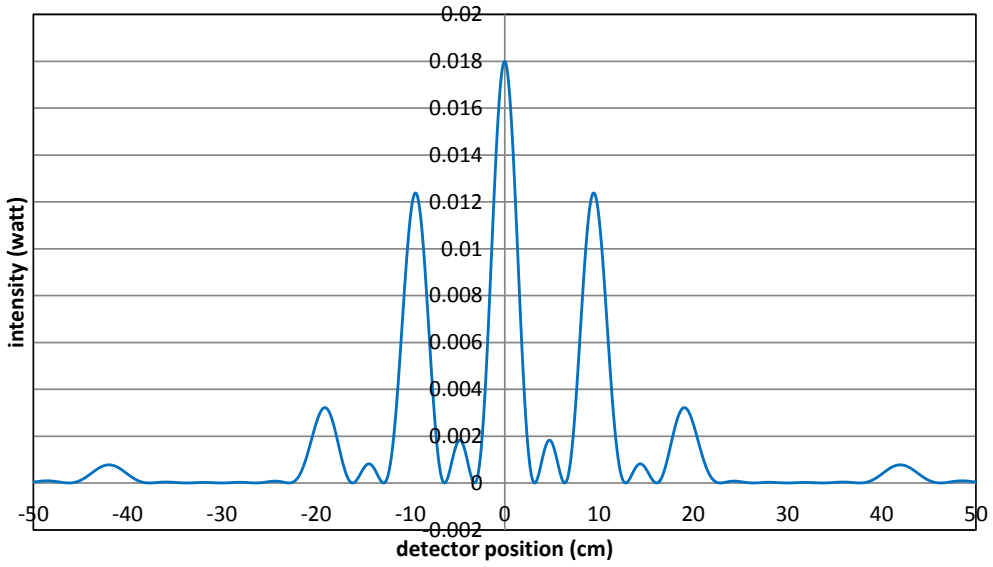

Figure 3.10: Triple-slit interference pattern using the sinc-function formula

The kappa variation calculated similarly looks as follows.

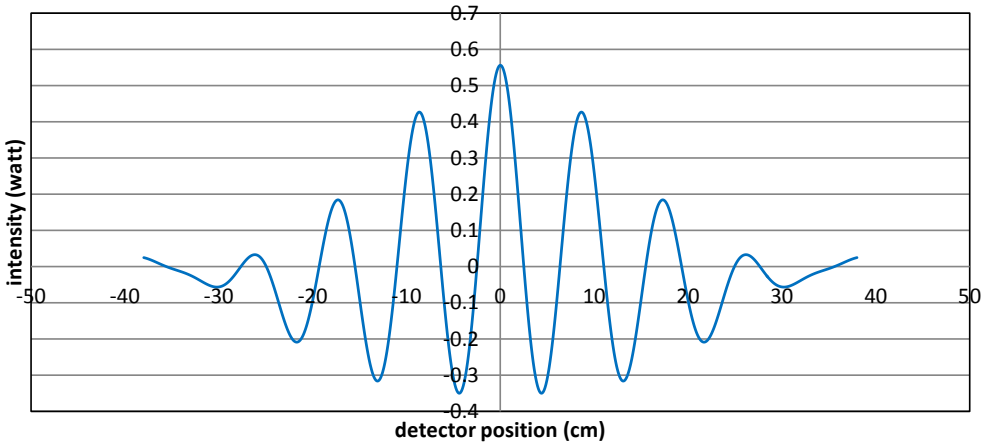

Figure 3.11: κ variation pattern resulting from the sinc-function formula

Although we have changed the wavelength, everything has been scaled down too, so we expect no effect on the interference pattern. And yet we observe that both the graphs look slightly different from our previously obtained graphs. The reason is that this simulation is about slits while the previous simulations were about slots. Although Babinet's Principle predicts that both slits and slots should give us the same graph if we are sufficiently far away, we realised that the distance required for such convergence in the case of our experiment is too high to be of practical importance. Although the program did prove to be a good quick first approximation to whether certain values for parameters would work, we cannot utilise the convergence suggested by Babinet to our advantage in these experiments.

3.3.2 Double-Slot Interference at available frequencies: 1GHz - 3GHz

We were limited by experimental resources and expertise, so we couldn't go up to a frequency as high as 15GHz. In spite of our target of 15GHz frequency, we carried on our experiments with the immediately available frequencies (1GHz-3GHz) in order to familiarise ourselves with the experimental requirements. Although we had signal generators that went up to 6GHz, we had to wait for a while before we got an antenna that could radiate at that frequency and another one that could detect at that frequency. We also had access to two microwave absorbers (which we used as slots) of dimensions 30.5cm $\times$ 30.5cm. We thus started with a double-slot experiment and tried to simulate the situation for this new configuration.

Following is the double-slot graph in WIPL-D at 1GHz, with the parameters: slot=30.5cm × 30.5cm, inter-slot distance=83cm, antenna-to-slot distance=519cm.

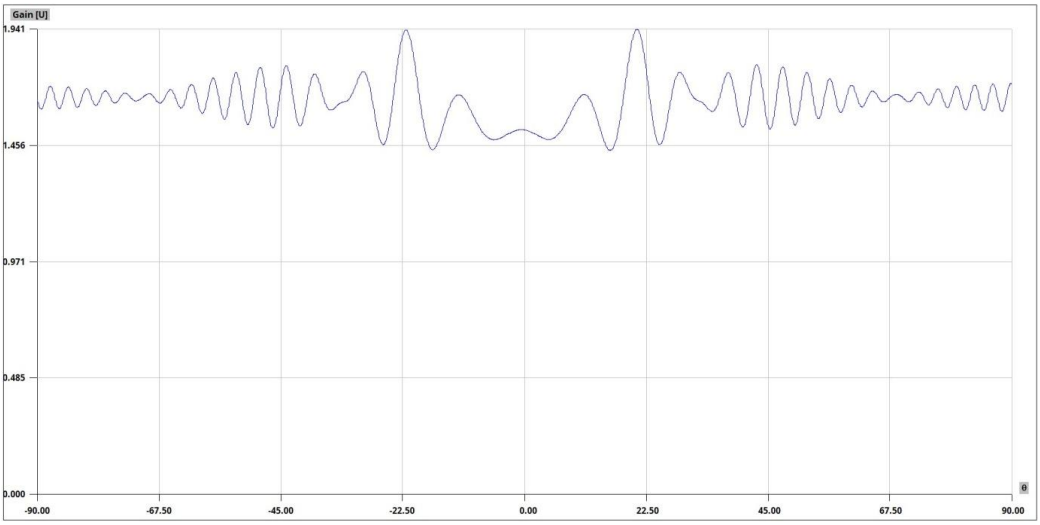

Figure 3.12: Double-slot interference pattern using WIPL-D with our experimental parameters

In this experiment, the slot-to-detector distance was 477cm . Observe that because of the chosen experimental parameters the interference pattern looks very different from a typical double-slot interference pattern. However, it matches well with our experimental observation.

We have also simulated with the same parameters for near field. However, WIPL-D uses certain assumptions in its calculations which are different for near field and far field, therefore it is difficult to predict which assumptions will be more suited for a particular set of dimensions. With experience, however, one realises which approximation will be better for a certain configuration. Near field assumptions are usually limited to very small distances from the slots.

3.3.3 WIPL-D Simulations at 6GHz

With newfound access to plate dipole antennas and a signal generator that can go up to 6GHz, we repeated the triple-slot experiment at this frequency. The slots were made of aluminium and their width was made smaller in order to bring the far-field closer. Simulations were run both in the near

field as well as far field. There was one problem, however, that we did not know the exact dimensions of the plate dipole antenna. These antennas were embedded inside thermocol, which we were not allowed to dismantle. Since our simulation assumes a half-wave dipole antenna source which is different from our plate dipole antenna, and since we couldn't incorporate the exact antenna dimensions in the simulation because we didn't have access to the information, our confidence level in the results weren't high. Therefore, we decided to write down a program in python, in such a way that it will be the antenna radiation that shall be sufficiently enough information fed to the simulation, without bothering about the antenna shape and dimensions. One could now even simulate point sources.

3.3.4 Python Simulations at 6GHz

We have used Huygen's principle to write a very simple code that has given us a lot of useful results. We are currently using this code to predict the outcome of our experiments.

The plan was to measure the antenna radiation pattern, or predict it from antenna dimensions or WIPL-D simulations, and then feed it to the program, which would use Huygen's principle to propagate the electromagnetic waves. However, point source assumption gave us sufficiently good results that matched closely with experiment.

Following are the results of this simulation at 6GHz (λ=5cm) with parameters: slot-width=12cm, slot-to-slot distance=30cm, antenna-to-slot distance=120cm, slot-to-detector distance=60cm, slot length=30cm.

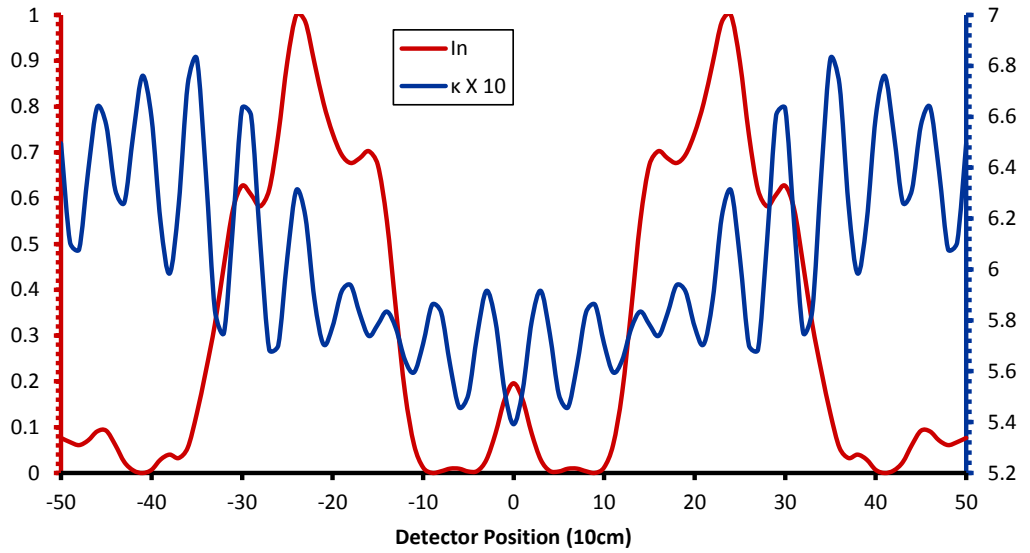

Figure 3.13: Plot simulated using Huygen's Principle. The triple-slot interference pattern is in red, in terms of dimensionless normalised intensity, while the plot for κ variation is in blue and multiplied by a scale of ten.

In this plot, I_n is the normalised intensity of a point in the triple-slot interference pattern. The results for the slit case instead of the slot case, parameters remaining the same, gives the following.

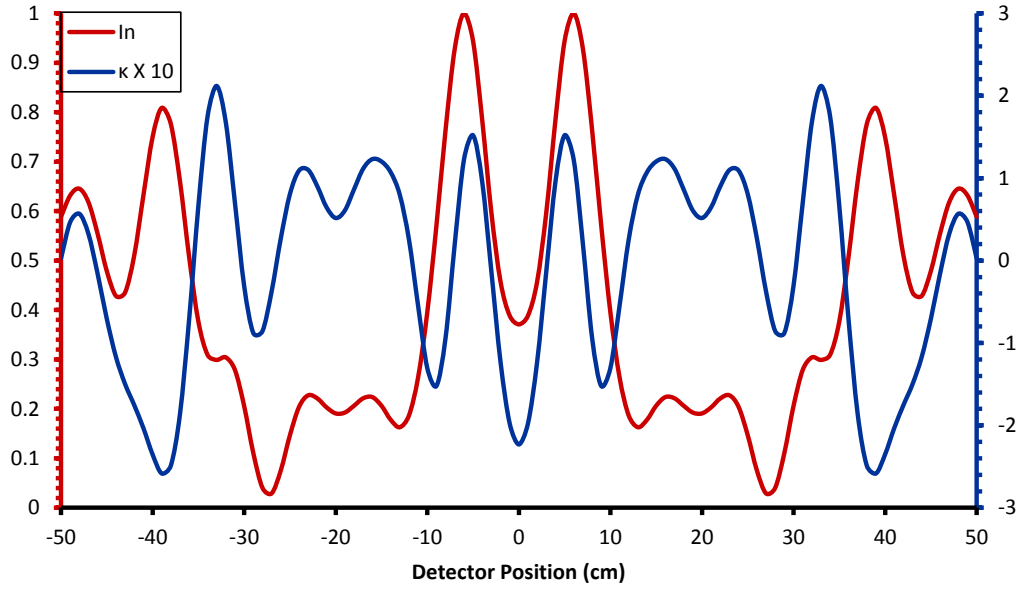

Figure 3.14: Plot simulated using Huygen's Principle. The triple-slit interference pattern is in red, in terms of dimensionless normalised intensity, while the plot for κ variation is in blue and multiplied by a scale of ten.

We infer from Fig. 3.13 and Fig. 3.14 that, if we can perform successful measurements in the far field, the above parameters can give a high value of κ, which is just one order of magnitude smaller that the intensities recorded by the detector due to interference.

An important point to note is that Huygen's Propagator, $\frac{e^{ik}}{r}$ involves the Eikonal Approximation (see Sec. 2.1.1). Therefore, using it to predict outcomes when we are too near field could be slightly tricky. One could improve this either by using mathematical tools like Method of Characteristics, or converging approximation methods like Multiple Multi-pole method.

3.3.5 Finite Difference Time Domain (FDTD) Method

We were initially considering this method to predict the interference pattern and kappa but we abandoned it because of very high computational cost. In *Hans de Raedt et al., 2011*, FDTD method was used by very efficient computers in order to calculate the interference pattern by solving Maxwell's equations for slits as boundary value problems. This is a time-domain method used for modelling computational electrodynamics. In this

method, time-dependent Maxwell's equations are discretised using central difference approximations to the space and time partial derivatives. The resulting finite-difference equations are solved in a leapfrog manner: the electric field vector components in a volume of space are solved at a given instant in time; then the magnetic field vector components in the same spatial volume are solved at the next instant in time; and the process is repeated over and over again until the desired transient or steady-state electromagnetic field behaviour is fully evolved.

3.4 WIPL-D Simulations for Construction of New Antennas

We ran some simulations in order to check if the antennas we wanted to construct would radiate the way we expected, based on their structure, design and dimensions.

The plate antennas we had used in the prior experiments were not very accurate. We wanted to make a more precise and perfect antenna, with high symmetry and resonance, and low return loss. After speculating on various resonant structures we decided up on a sleeve-dipole antenna.

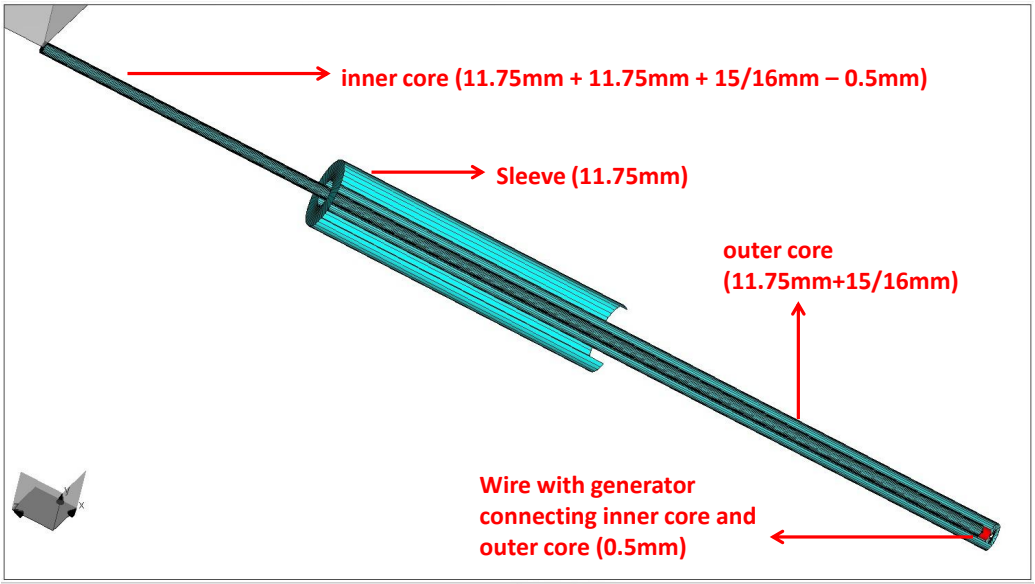

Figure 3.15: Simulation of sleeve dipole antenna in WIPL-D

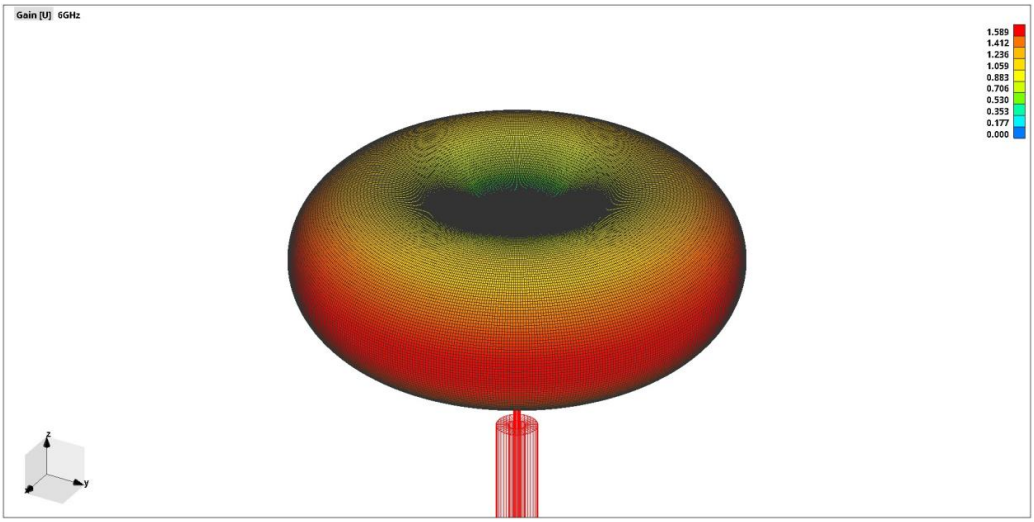

Figure 3.16: Antenna radiation pattern of a sleeve dipole antenna. Observe the close resemblance to that of a normal dipole antenna.

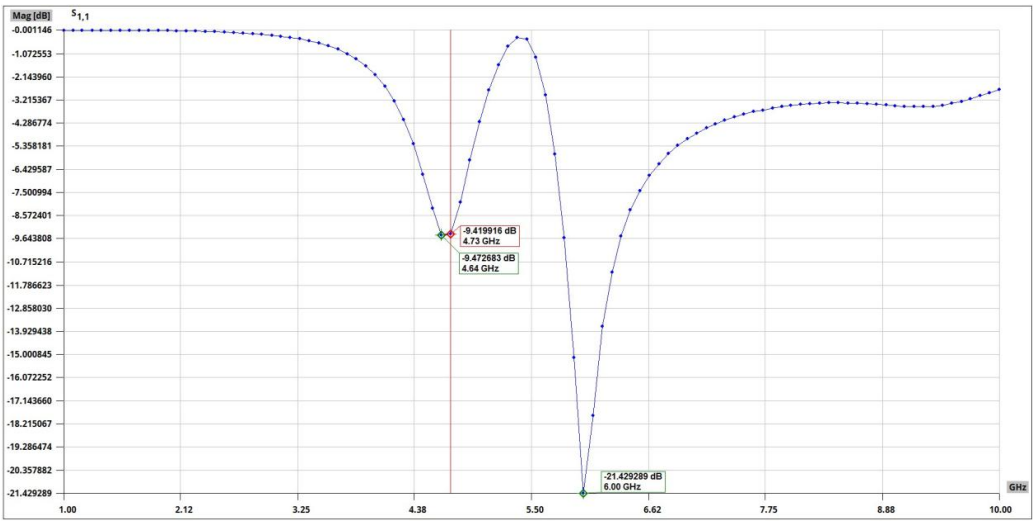

Figure 3.17: Return Loss graph plotted from the simulated sleeve dipole antenna.An absolute minimum peak at 6GHz shows that this structure is highly resonating at 6GHz.

The dimensions we decided upon gave us a very low value for return loss at 6GHz, which means our structure resonates at 6GHz giving us a stronger and more precise signal at this frequency.

Chapter 4

Experimental Methods

The aim of our experiment is to get a highly precise triple-slot interference pattern in the microwave regime, at around 6GHz. In this low frequency regime, the wavelength and other dimensions are in the centimetre scale and can be considered macroscopic. Such experiments have not been performed before. We took a step-by-step approach to gradually build the accuracy of our experimental set-up. Although we haven't yet reached the level of precision required to observe a value as small as κ, we have troubleshooted practical problems at every stage of the experiment and we have got some useful results to ponder upon.

4.1 Components

The basic set-up of our experiment is conceptually simple: we require a source, a slot-screen and a detector. Of course, when it comes to practical realisation of an experiment, many other requirements and considerations enter into the picture. Here are some of the important components in our experiment.

4.1.1 Microwave Source and Transmitter

To generate microwaves we used a microwave signal generator, Anapico APSIN6010, which is an analogue signal generator.These microwaves generated are transmitted by an antenna connected to the signal generator via cable. In our experiments so far, we have either used half-wave dipole antenna (1GHz) or plate dipole antenna (up to 6GHz) or sleeve dipole antenna (6GHz).

4.1.2 Microwave Absorbers

In order to make slots that would block microwaves as perfectly as possible, initially we used sheets of 30.5cm $\times$ 30.5cm Eccosorb polymer. This is a thin, flexible, electrically non-conductive silicone rubber sheet that absorbs microwaves in the frequency range 800 MHz to 18GHz by the principle of dampening cavity resonance. In our later experiments we cut out slots of 3mm thick Aluminium (12cm $\times$ 30cm). The skin depth of Aluminium at 1GHz is 2.5932 μm and at 6GHz is 1.0587 μm, therefore 3mm is many many times thick enough to block electromagnetic waves at these frequencies. In an attempt to avoid too much reflection from the aluminium slots which would otherwise contribute to return loss, the slots were covered in black paper.

Finally, we concluded that the best way to make these slots at the moment is to cover the cut out aluminium slots with the Eccosorb polymer. This would prevent the microwave reflection as well as transmission (if the slots behaved like secondary antennas). If there is still some scope for improvement, we can perhaps connect the slots to a circulator that would prevent the build-up of any electromagnetic fields at the slots.

4.1.3 Microwave Detectors and Pre-amplifiers

Due to huge amount of space loss, pre-amplification is necessary for accurate detection of microwave intensity. We had a pre-amplifier that could amplify signals of up to 3GHz. At these frequencies, we used a loop probe (loop antenna) for the purpose of detecting microwave intensity. In the absence of pre-amplification at higher frequencies, we required two highly resonant antennas at the same orientation to act as transmitter and receiver. This was accomplished using plate dipole antennas and sleeve dipole antennas.

4.1.4 Spectrum Analyser and Network Analyser

The detector was directly connected to an N9915A FieldFox Handheld Microwave Combination Analyzer which shows the intensity reading in the Spectrum Analyser mode. The Microwave Analyser has got other modes too, like Network Analyser mode and Vector Voltmeter mode that are very useful in vector measurement of fields, that is, measuring both magnitude as well as direction of the field.

4.1.5 Stationary and Movable Stands

In interference experiments, it is very important to make sure that other objects in the experimental set-up don't contribute to the resultant interference pattern. Cables don't contribute since they are heavily insulated. The stands for the antenna, detector and slots, however, may contribute significantly if care is not taken to cancel out their effect in some way. One of the best ways is to build them out of materials that are transparent to microwaves, especially in the 1GHz-6GHz range. We tested certain materials and concluded that card-board and thermocol (trade name for polystyrene in India) were totally transparent to this frequency range, and decided to build slot stands out of them. The stand for the transmitting and receiving antennas may be overlooked since we can always arrange to have the stand in the null point of an antenna, but the slot stands have to be made out of this material. We made slot stands out of both cardboard as well as thermocol.
For the purpose of detection along a straight line, we require a stand capable of moving along this line as precisely as possible and without affecting the interference pattern. We haven't yet been able to design the perfect stand for this purpose, although we have designed many different stands during the course of our experiment.

4.1.6 Anechoic Chamber

Our experiment relies heavily on precision, so the use of an anechoic chamber is inevitable. The anechoic chamber is a room whose surfaces are totally covered with microwave absorbers. In other words, it is equivalent to a dark room in an optics experiment. By shielding the experiment from the outside world and preventing reflections inside, the anechoic chamber can greatly increase the accuracy of our experiment. Although we haven't yet performed any experiments in an anechoic chamber, we might consider the option in the near future.

4.2 Experiments

Many experiments were designed and performed in order to understand the experimental requirements of this regime. Following are some of the important experiments we performed. The result of every experiment brought us closer to a better experimental design.

4.2.1 Characterisation of Dipole Antenna at 1GHz

We experimentally plotted the antenna pattern of a half-wave dipole at 1 GHz. The experimental set-up was simple and consisted of the antenna propped up on a rotatable stand with a compass and the loop probe detector fixed on to another stand at a distance of 2.7m from the antenna. The antenna was connected to the Signal Generator and the detector was connected to a pre-amplifier, and through it to the Spectrum Analyser via cables.

We set the input frequency provided by the signal generator to 1 GHz at a power of 10 dBm, and measured the antenna output as recorded by the detector at every 10 degrees rotated by the antenna from 0 to 360 degrees. The antenna was rotated with the help of the rotatable stand and the angle of rotation was directly read off a compass fixed to the same stand which rotated along with the antenna. Here is a schematic of the experimental set-up.

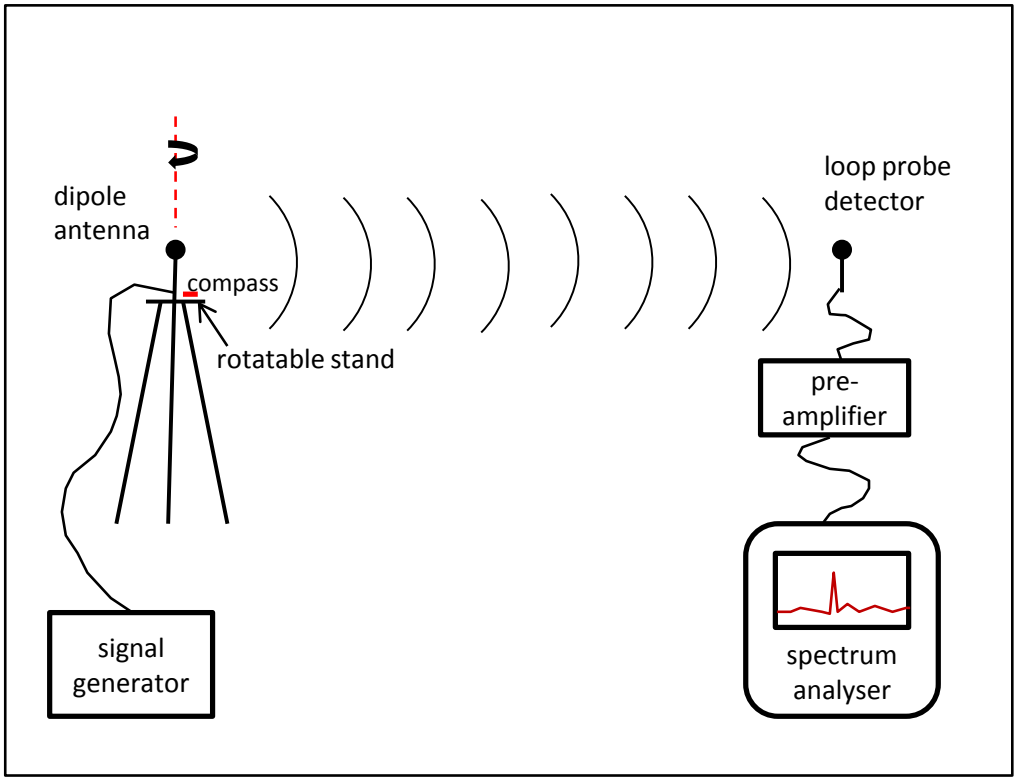

Figure 4.1: A schematic of the experimental set-up that was used to measure the antenna radiation pattern.

We also checked how the power radiated fell with the distance due to

space loss by manually moving the dipole antenna stand along a calibrated straight line drawn on the floor. As the antenna-to-detector distance was increased, the intensity measured by the loop probe detector was recorded.

4.2.2 Double-Slot interference at 1GHz and 2GHz

We used the same dipole antenna to perform a double-slot experiment at 1GHz and 2GHz. Although this antenna doesn't behave like a half-wave dipole at 2GHz, it's still a dipole and hence similar radiation pattern but with reduced efficiency. The antenna was mounted on the same stand. The slots were made out of Eccosorb sheets fixed on to a large piece of strong blue Dow polymer with some wood for support. Once again the loop probe detector was used for detection. The probe was moved manually over a calibrated line drawn on the wall opposite to the antenna and the slots. We performed the experiment with various different parameters.

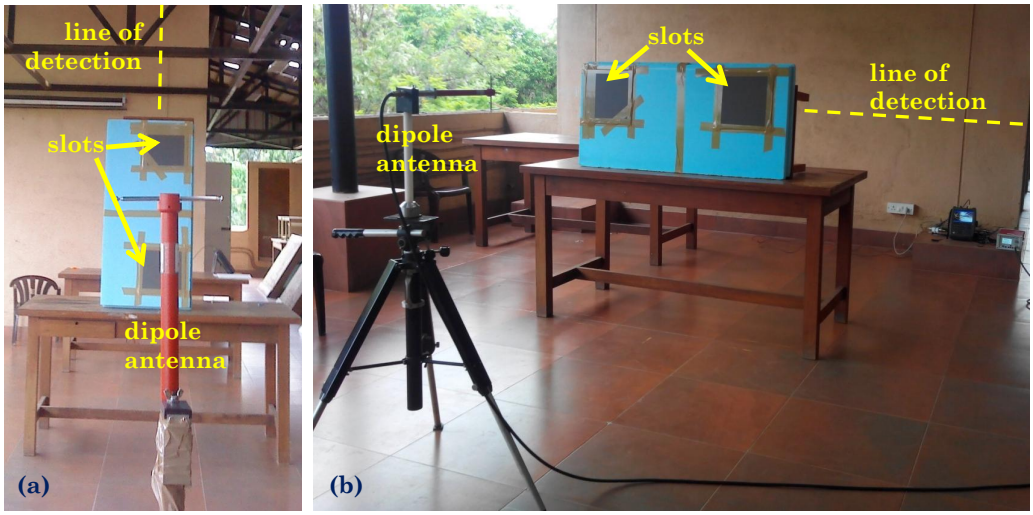

Figure 4.2: The 'antenna plus slots' system can be arranged in two ways: (a)vertical and (b) horizontal. The arrangement (b) is preferred over (a) because the ground reflection is uniform over the entire range of detection, whereas in case of (a) the ground reflection is different at different points of detection.

Initially, we were detecting in the vertical plane. However, this arrangement introduced the problem that the ground reflection was different at dif-

ferent points of detection due to different height from the ground at every point. Therefore we shifted to a horizontal arrangement of the slots, so that detection was performed in the horizontal plane and the effect of ground reflection was the same at every point of detection, eliminating the asymmetry.

4.2.3 Characterisation of Plate Antenna at 6GHz

Students of the radio-astronomy department fabricated a plate antenna whose radiation pattern at 6GHz is similar to that of a dipole antenna. We decided to use this antenna in our experiment. Here is a basic schematic of this antenna.

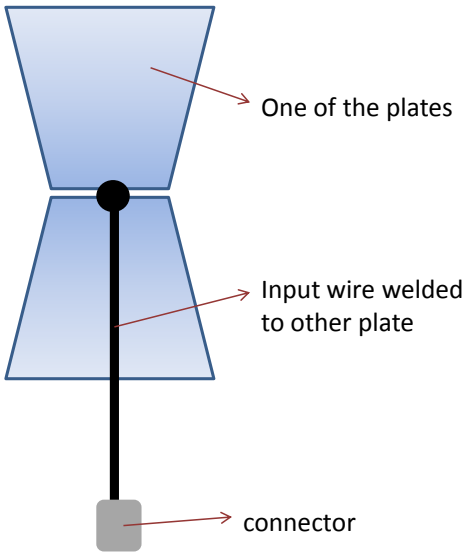

Figure 4.3: A schematic of the plate antenna fabricated in the radioastronomylab, for trasnmitting at 6GHz.

The dimensions of this antenna are unknown since it was embedded inside a thermocol packing which we were forbidden from removing. It was roughly estimated to be around 46mm. The antenna was directly fixed to the signal generator via a connector.

We used the same set-up as in the case of characterisation of the 1GHz half-wave dipole antenna in order to characterise this antenna too. We measured the antenna radiation pattern as well as the variation in radiated intensity with increasing distance from the antenna.

4.2.4 Double-Slot interference at 1GHz, 2GHz, 3GHz and 6GHz

Just like in the case of the dipole antenna, we used the same arrangement to perform double-slot experiment with the source being the plate antenna. Detection was done in the horizontal plane.

For up to 3GHz, we used the loop probe detector for the purpose of interference pattern measurement just like before. But beyond 3GHz the pre-amplifier wouldn't function and the received intensity recorded by the loop probe without the help of pre-amplifier was almost negligible. At 6GHz, therefore, the detecting antenna being used was not a loop probe but another identical plate antenna directly connected to the Spectrum Analyser, and at the same orientation (polarisation) as the transmitter antenna. This method is more accurate as well as more sensitive because there is no power loss due to polarisation mismatch between the transmitter and the receiver antennas.

Since detection had to be performed with a similar plate antenna and not a loop probe, we had to devise a method of detection slightly different than before because this plate antenna is too delicate to be moved around like the loop probe. In the new arrangement, the line of measurement would now be along the edge of a long table. We fixed a measuring tape along this edge. The detector plate antenna connected to the spectrum analyser was stably placed on a movable chair. This chair was carefully moved along the table every 10cm to measure the microwave intensity received, making sure always that the flat vertical surface of the chair is in contact with the edge of the table so that the chair moves exactly along a straight line without rotating. This arrangement of detection was much better than before since the manual effort was less, and so was the human error.

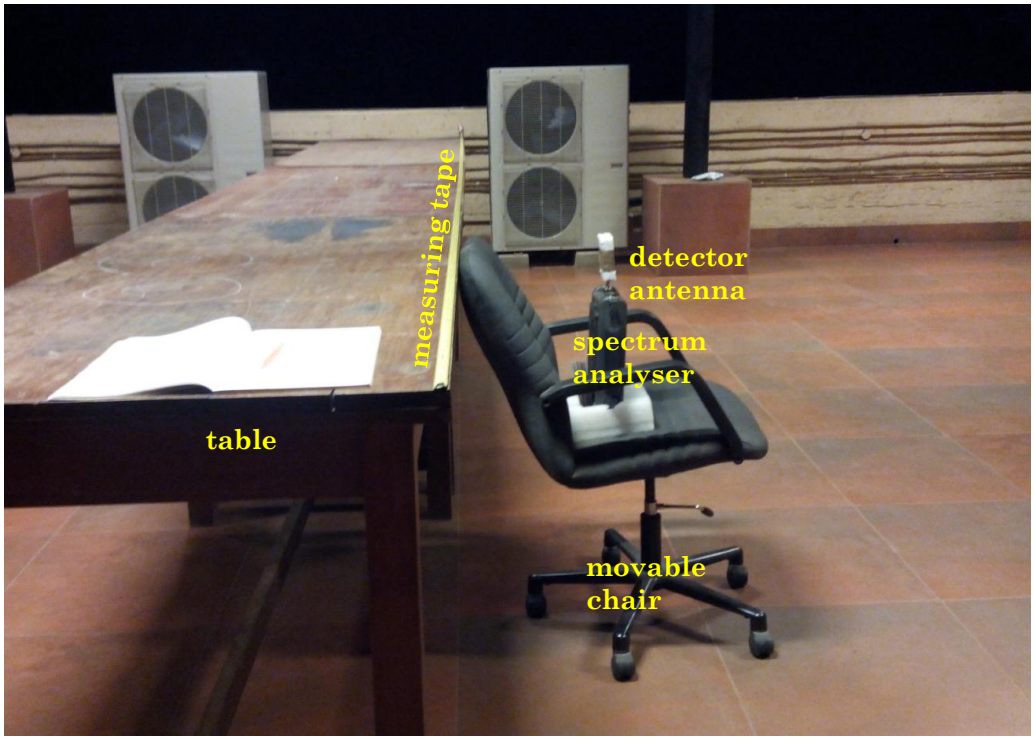

Figure 4.4: A new method for antenna radiation pattern detection.

From the experiment described in the next section, we realised that wood and blue Dow polymer aren't completely transparent to 6GHz (although they are very transparent at slightly lower frequencies), therefore using them as support for fixing the slots was a huge mistake. Therefore, in our later experiments we made slot stands out of white thermocol, which is transparent to 6GHz. To make a slot stand, thermocol was cut into a rectangular shape and a thin slice was cut into it, inside which one could fix a slot. We also placed some microwave-absorbing Eccosorb sheets at crucial spots on the ground in order to minimise the ground reflection.

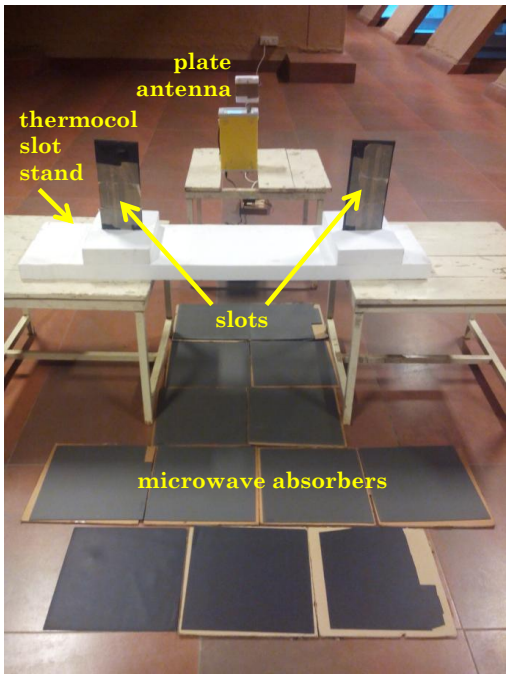

Figure 4.5: An illustration of the double-slot experimental set-up at 6GHz.

A point to note is that the stools used in the experiment to prop up the source, detector and the slots, were made of wood and metal. However, they hardly had any influence on the interference pattern, as checked by recording the antenna radiation pattern both in the presence and absence of these stools.

4.2.5 Determination of microwave transparency of materials at 6GHz

It is important to understand which materials are suitable for making stands in our experiment so that they themselves don't diffract the microwaves and hence contribute to the slit-interference pattern. Our experiment is a precision experiment which looks at a value whose magnitude is at least three orders smaller than that of the intensity peak of the triple-slot interference pattern. Under these circumstances, it becomes extremely crucial to keep the error at least one order below this threshold magnitude.

We set-up a simple experiment that allowed us to check how various materials were behaving with the microwaves; it was more of a qualitative test for transparency. In the set-up, we basically placed a sheet of the material to be tested between the transmitter and the receiver antennas (the plate anten-

nas at 6GHz). We initially recorded the interference pattern caused due to our experimental set-up consisting of two metallic stools placed one over the other over a short distance range, in the absence of the material to be tested. We compared this to the interference pattern recorded in the presence of the material. If the material was highly transparent, it would have no effect on the interference pattern. On the other hand, a material highly opaque to microwaves would cause the detector to record a significantly lower intensity. Everything else would just modify the intensity pattern but we need not concern ourselves with them. The transparent materials would be considered for making the stands while the opaque materials would be considered for making the slots. Card-board and thermocol were the most transparent whereas 3mm thick aluminium and the microwave absorbers were completely opaque. A thin sheet of PVC also seemed to be almost transparent.

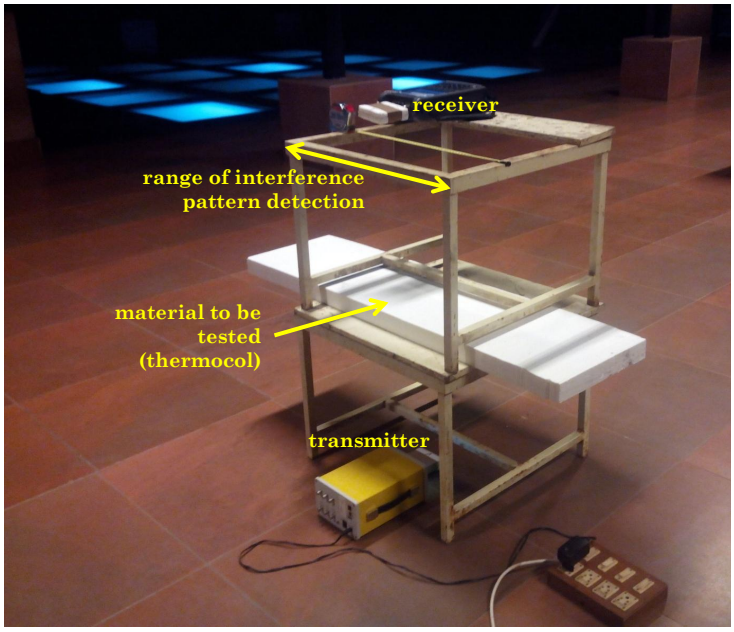

Figure 4.6: An experimental set-up in order to qualitatively assess the microwave transparency of cerain materials at 6GHz.

4.2.6 Differential Measurement of interference pattern at 6GHz

Our experiments were not giving us satisfactory results, so we decided to do a differential measurement instead of the conventional intensity measurement. In the case of differential measurement, one compares the rate of change of a value and not the value itself. This is more accurate because values have

small magnitudes and they may get lost or drowned in the noise, or there might be errors getting added to them. So when we look at the rate of change instead of the magnitude of the values measured themselves, consistent errors in the magnitude of the values get cancelled out, therefore giving us a more precise and trustable plot.

The experiments involving differential measurement were performed in the open fields in the Radio Observatory at Gauribidanur. We chose this spot since the location is quite isolated, so we expected less external disturbance, and group members of the Radio-astronomy lab we have collaborated with often come here to perform experiments of their own. We performed both single-slot and double-slot interference experiments in the Near Field. These experiments were not what we conventionally mean by slot-interference experiments, however. We kept the position of the detecting antenna constant, and also that of the slots, but we moved the source along a line. This was done because it was very convenient in our setting to move the source instead of the detector. We would, of course, not get a slot-interference pattern but we would surely get some sort of interference pattern which we could compare with a theory that simulates the same situation in order to evaluate how well this method works. If the results are decent, we can go ahead and make the requisite change in the experimental setting in order to perform a double-slot interference pattern measurement using this method.

The set-up of these experiments were very similar to the previous set-ups, except for the fact that we were using chairs, PVC pipes and bricks instead of tables, as we can see in the following picture. We could not move the detecting antenna because in the absence of the movable chair at Gauribidanur, the Spectrum Analyser it was attached to could not be held stably in a vertical position while moving it. The signal generator, on the other hand, could comfortably stand on a stool that was moved exactly in a horizontal line as ensured by the PVC pipes.

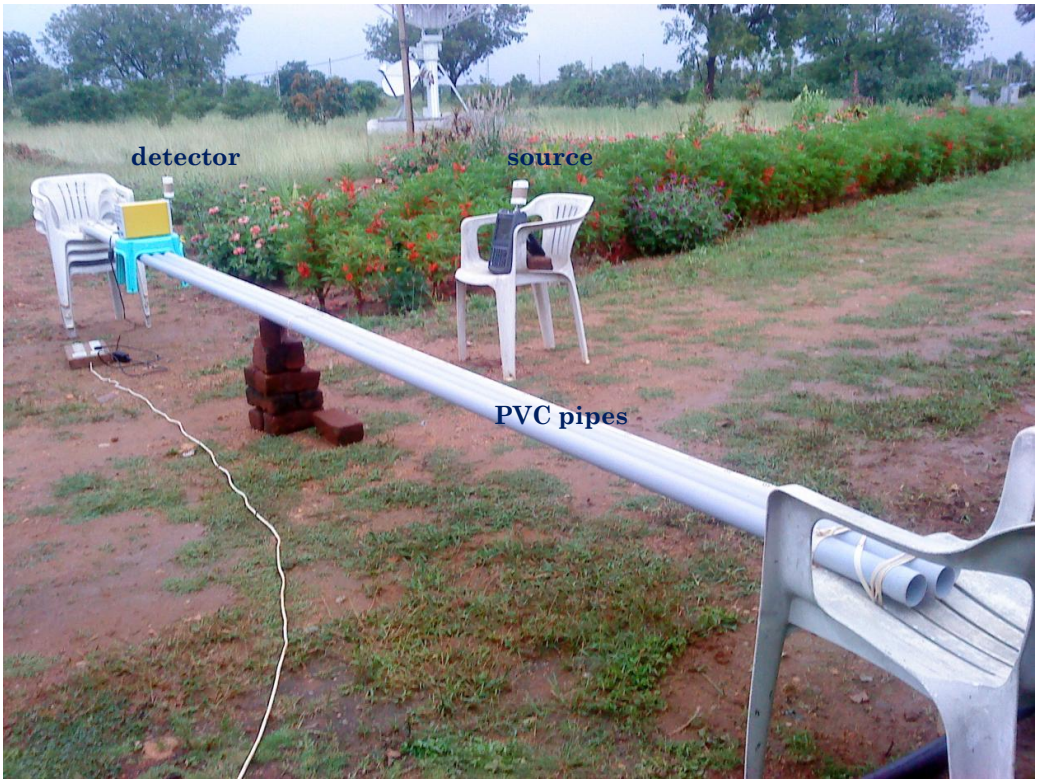

Figure 4.7: The experimental set-up at Gauribidanur.

While measuring the interference pattern, the slots were placed on thermocol stand, which was again held with the help of plastic chairs. At every point of measurement, three readings were taken:
(1) A= with slots
(2) B=without slots
(3) C=with slots once again.
An average D of the first and third readings was taken.

$$D = \frac{A + C}{2} \tag{4.1}$$

The differential measurement M at the point was given by:

$$M = \frac{B - D}{B + D} \tag{4.2}$$

The observed results matched with theory, as we can see in Fig. 5.32 and Fig. 5.33, but the precision was very low since we were manually moving the source. We look forward to the involvement of greater mechanisation in the detection process.

4.2.7 Construction of the Quarter-Wavelength Choke-Sleeve Dipole Antenna at 6GHz

In order to increase the precision of our experiment, we wanted to increase the efficiency and precision of the power transmitted by the source antenna. We did a literature review of various highly resonant structures that we could use in our experiment for constructing very sensitive antennas. We decided to construct a QWCS antenna, also referred to as sleeve dipole antenna, at 6GHz (see Sec. 2.3.3).

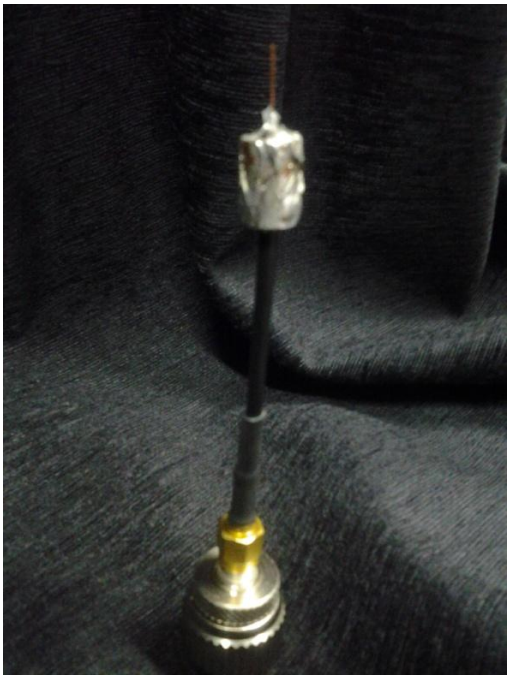

Figure 4.8: A sleeve dipole antenna we have constructed.The structure is highly resonating at 6GHz.

The antennas we have constructed are functioning decently at 6 GHz with 12mm as the quarter-wavelength. We have used the coaxial cable RG174 for antenna construction. The coaxial cable is stripped to expose the outer conductor or 'braid', which basically consists of wires braided to form a cylinder. Stripping is done up to a length of half-wavelength of the electromagnetic wave we want to use this antenna to generate/receive (resonant frequency). Carefully, using a sharp object, this structure is 'unbraided' and individual strands in the braid are separated for up to a length of quarter-wavelength, thus exposing the same length of insulator inside it that protects the inner conductor. This braid is folded backwards symmetrically in order to form a

sleeve, which is soldered to the outer surface a cylindrical copper structure that fits like a sleeve on the wire. This gives continuity to the structure. Soldering is the most difficult step here because of the small dimensions involved, the tendency of PVCs to melt, impurities on surfaces and the high precision required. Once the soldering cools down the insulator surrounding the inner wire can be cut and pulled out to expose this inner wire. This exposed inner wire, along with the outer sleeve, is going to generate the electromagnetic waves.

Thermocol has been filled inside the sleeve for extra support. The resultant antenna radiation pattern is in accordance to our expectations, although not as symmetric. Errors are attributed to lack of smoothness and symmetry due to imperfect soldering.

4.2.8 VSWR and Return Loss Measurement at 6GHz

The Network Analyser mode of the Microwave Analyser allows one to directly read off the S11 parameter in terms of VSWR as well as in terms of Return Loss, upon connecting the concerned antenna at the input terminal. We measured the VSWR and Return Loss parameters of the plate antennas as well as the sleeve dipole antennas.

4.2.9 Vector Measurement at 6GHz

The Microwave Analyser has also got a Vector Voltmeter mode for carrying out vector measurements. Vector measurements constitute the relative amplitude and phase differences between two antennas, one of which is a source and the other is a detector. The source antenna is connected to the output terminal and the detector antenna is connected to the input terminal. The Microwave Analyser itself acts as a signal generator in this case, although the maximum output power is quite low (3dBm). The display consists of the relative amplitude and the relative phase measured by the detector antenna with respect to the source antenna. The units of measurement can be chosen according to convenience.

Vector measurements can be very useful for error analysis. Suppose we perform our experiment at lower frequencies, we cannot limit ourselves to the dimensions of an anechoic chamber. In such a scenario, we will have to perform our experiment in an open field and characterise all the possible sources of error in the field, including reflections, ground reflections and space loss. These reflected waves will not just add or subtract with the interfering waves in our experiment, but also interfere with them in accordance to the principle of superposition. Both amplitude as well as phase will get affected. Vector

measurements allow us to know these effects and to cancel them out during our analysis. We are currently performing some vector measurements.

Chapter 5

Results and Discussion

5.1 Characterisation of Dipole Antenna at 1GHz

5.1.1 Radiation Pattern of Dipole Antenna

Initially, we started working with a 1 GHz half-wave dipole antenna, so we experimentally plotted its antenna pattern representing a plane that bisects the antenna perpendicular to its arms. The following plots are in dBm units, the transmitted power being 10dBm and the detection being done at a distance of 2.7m. (Fresnel Number = 0.0277)

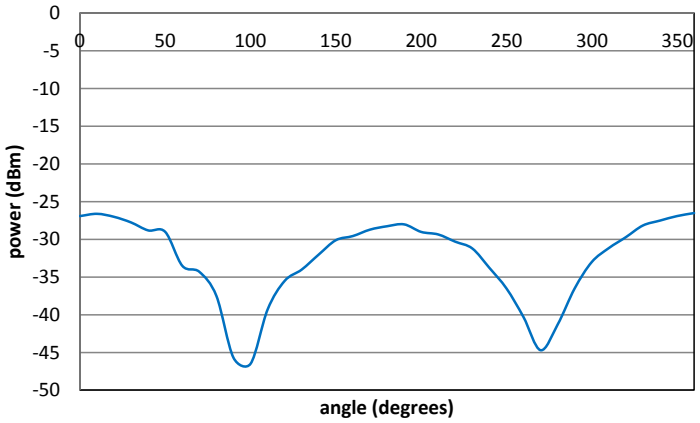

Figure 5.1: Antenna radiation pattern of half-wave dipole antenna from experiment.

The antenna radiation pattern was also radially plotted, on a scale translated in order to exclude negative numbers on the axis. The shape of this

plot aligns with our expectations, as can be seen from its close resemblance to the theoretical plot derived from WIPL-D.

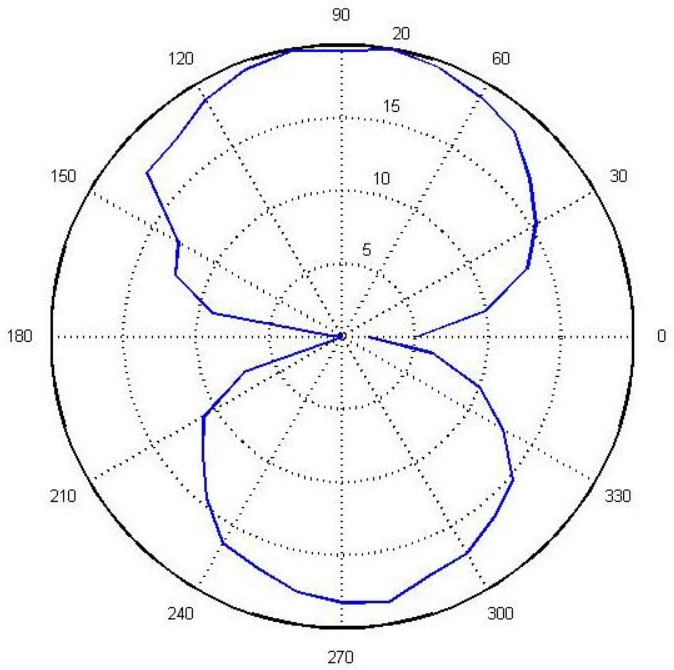

Figure 5.2: Radial plot of antenna radiation pattern of half-wave dipole antenna from experiment.

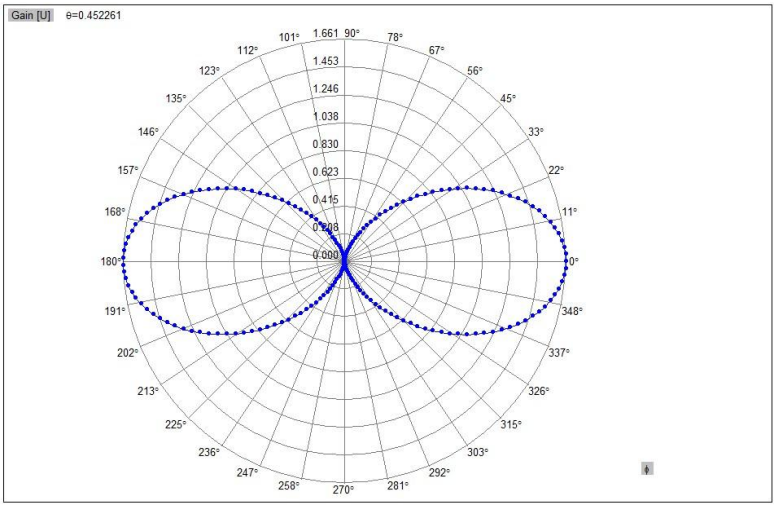

Figure 5.3: Theoretical plot for antenna radiation pattern of half-wave dipole antenna in WIPL-D.

5.1.2 Fall in Radiation Intensity with Distance

We also plotted the way the power radiated fell with the distance of detection. Here is a plot of the same; the power transmitted being 13 dBm, and measurement carried out up to a distance of 21 feet. Looking at the trendline of the plot we can say that the radiated power falls off as square of the distance, as expected.

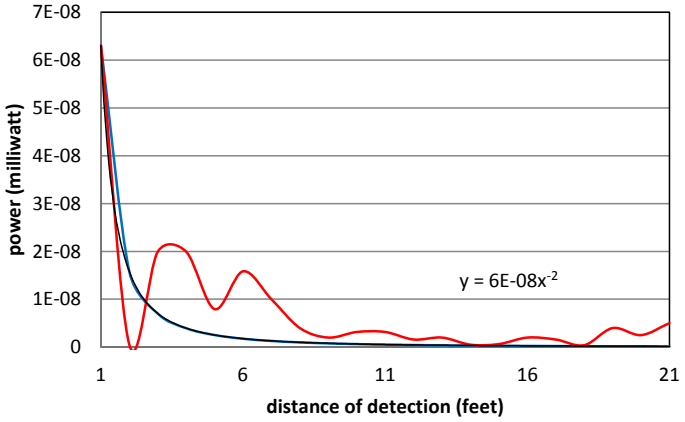

Figure 5.4: Fall in received electromagnetic intensity (red) as compared to the $\frac{1}{r^2}$ fall in intensity (blue) that is expected with increasing distance from the transmitter antenna (half-wave dipole antenna). We had set the input frequency provided by the signal generator to 1 GHz at a power of 13 dBm.

5.2 Double-Slot Experiments using Dipole Antenna source at 1GHz and 2GHz

5.2.1 Vertical Slot Arrangement at 1GHz

In the first double-slot experiment at 1 GHz, the slots were arranged vertically. These are the plots resulting from the parameters: antenna-to-slot distance = 5.19m, slot-to-slot distance = 83cm, slot width = 30.5cm, slot-to-detector distance = 4.77m, power transmitted = 10dBm. The units used are milliwatts. (Fresnel Number for diffraction at slots= 0.01445, Fresnel Number at interference pattern detection = 0.01625). Both the theoretical and experimental plots represent the same range of measurement. In comparing them, we look only at the shape of the interference pattern and not at the absolute values of power, because the low efficiency of antenna radiation and high free-space loss significantly reduces the intensity measured at the detector during the experiment, as compared to the theory. The double-slot pattern we recorded was very distorted as compared to the expected double-slot pattern calculated from WIPL-D using the same parameters and we suspect that ground reflection played a major role in this.

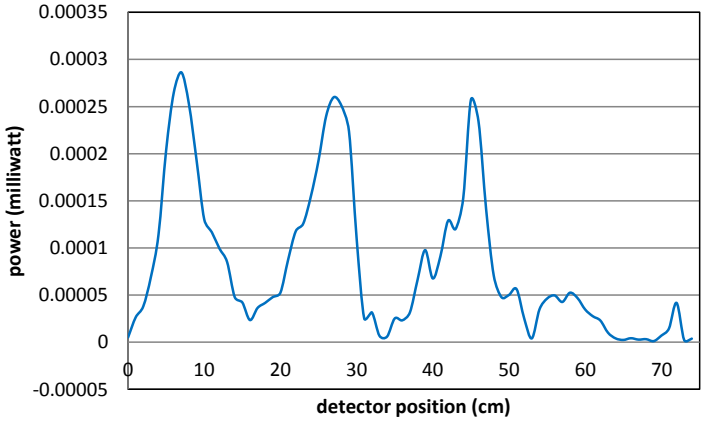

Figure 5.5: Double-slot interference pattern at 1GHz from experiment with vertical slot arrangement (transmitter=half-wave dipole antenna).

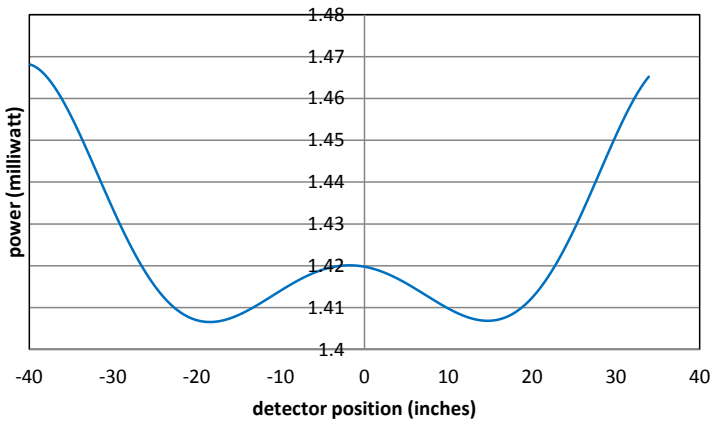

Figure 5.6: Theoretical plot for double-slot interference pattern at 1GHz in WIPL-D.

5.2.2 Horizontal Slot Arrangement at 1GHz

We then carried out the same experiment with the slots being placed in a horizontal line, the parameters being antenna-to-slot distance = 2.5m, slot-to-slot distance = 83cm, slot width = 30.5cm, slot-to-detector distance = 3m, power transmitted = 10dBm. The units used are milliwatts. (Fresnel Number for diffraction at slots= 0.03, Fresnel Number at interference pattern detection = 0.02584)

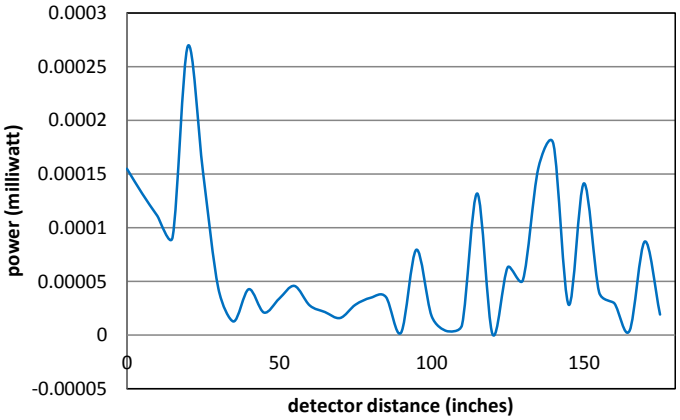

Figure 5.7: Double-slot interference pattern at 1GHz from experiment with horizontal slot arrangement (transmitter=half-wave dipole antenna).

The results in Fig. 5.7 did not match the theoratical expectation shown in Fig. 5.6. We attribute this to the crudeness of our experimental set-up, especially the loop probe (detector antenna) movement, and unknown environmental disturbances. The differences in the absolute values of intensities are understandably because of space loss, but the difference in the interference pattern shape suggested that there were more problems.

5.2.3 Horizontal Slot Arrangement at 2GHz

The same experiment was carried out once again but at a different frequency, that is, 2GHz. Note that at 2GHz, our antenna is still a dipole antenna but not a half-wave dipole. The parameters were: antenna-to-slot distance = 2.5m, slot-to-slot distance = 83cm, slot width = 30.5cm, slot-to-detector distance = 6m, power transmitted = 10dBm. The units used are milliwatts. Two sets of the same experiment were performed to check reproducibility. (Fresnel Number for diffraction at slots= 0.015, Fresnel Number at interference pattern detection = 0.02584)

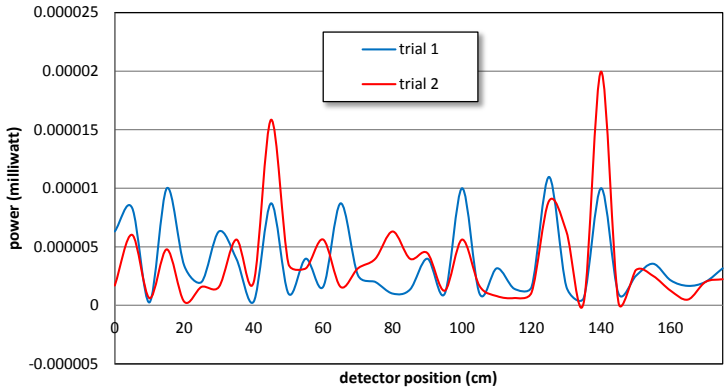

Figure 5.8: Double-slot interference pattern at 2GHz from two sets of experiment on the same day (transmitter=half-wave dipole antenna).

Although we did not get the expected interference pattern, it can be seen that the pattern measured is reproducible to a decent extent. Therefore, we concluded that the major drawback in our experiment was not the relatively large distances involved along with a small transmitted power, but consistent external disturbances from the surrounding environment.

5.3 Characterisation of Plate Antenna at 6GHz

5.3.1 Radiation Pattern of Plate Antenna

We wanted to go to higher frequencies, but we did not have a pre-amplifier that went higher than 3GHz. The 1GHz half-wave dipole antenna was not efficient at transmitting power at 6GHz, the loss was too high to record any signal without a pre-amplifier. Therefore, we procured some recently fabricated plate antennas from the radio-astronomy lab at RRI that would radiate more efficiently at 6GHz and decided to use them in our experiment. We experimentally plotted the antenna radiation pattern of the plate antennas at 6GHz. We expected it to be very similar to that of a typical dipole antenna.

Following is a radial plot of the antenna radiation pattern in dBm units, and translated suitably to avoid negative values. This was just to check the general antenna pattern. Detection was done at a distance of 250m (Fresnel Number = 0.016928). The pattern does resemble one of a typical dipole antenna.

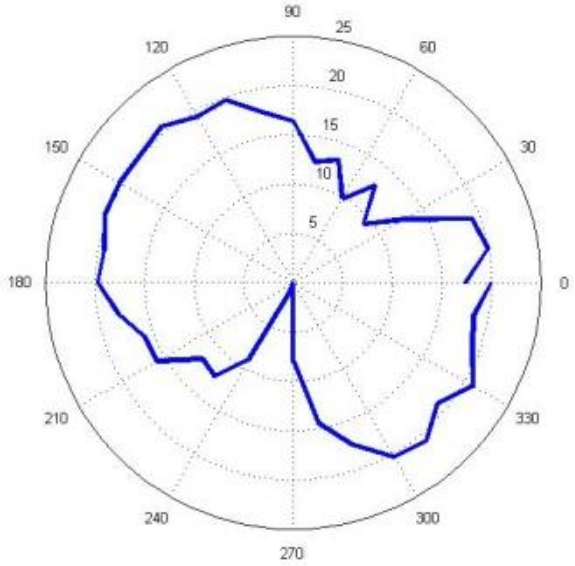

Figure 5.9: Antenna radiation pattern of plate dipole antenna from experiment.

We also performed some intensity pattern measurements along a straight line of detection, at various distances from the antenna. Here is a plot of the intensity pattern measured at 1m, 2m, 3m and 4m. We observed that the intensity fell off from the centre more rapidly than expected of a typical dipole antenna.

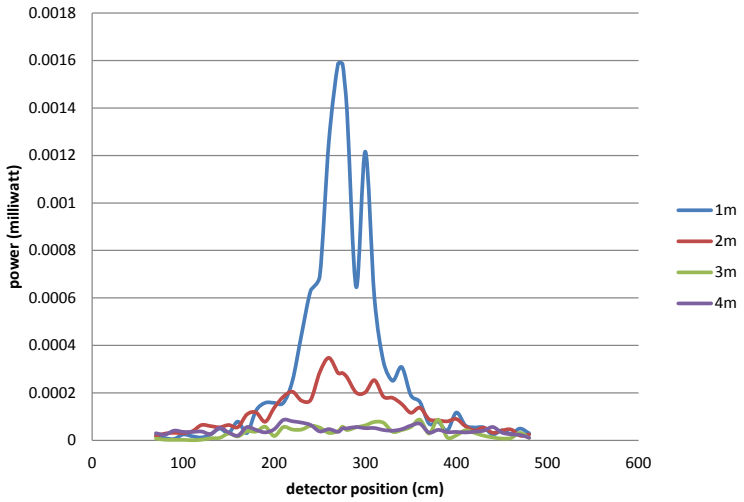

Figure 5.10: Antenna radiation pattern of plate dipole at different distances of detection.

5.3.2 Fall in Radiation Intensity with Distance

The plot of radiation intensity falling with radial distance from the transmitter antenna also seems to be much sharper. Intensity falls off as $\frac{1}{r^{2.5}}$ instead of the expected $\frac{1}{r^2}$ trend, as can be seen in the plot.

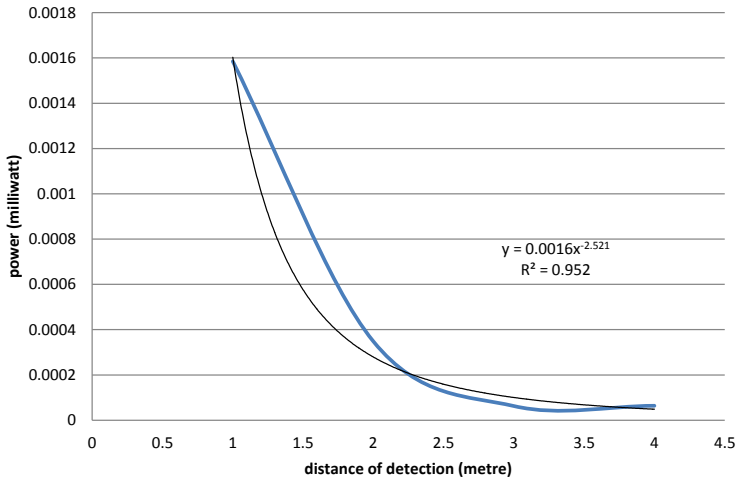

Figure 5.11: Fall in the received electromagnetic intensity upon moving further away from the transmitter antenna (plate dipole antenna).

Still, a decent resemblance with a typical dipole radiation pattern made us go ahead and perform some slot-diffraction experiments with these antennas, mainly to sort things out, like identify some practical requirements in such experiments and at such frequencies, before we went ahead for a better antenna.

5.4 Double-Slot Experiments using Plate Antenna source at 1GHz, 2GHz, 3GHz and 6GHz

Double-slot interference experiments were performed using the plate antenna as transmitter at 1GHz, 2GHz, 3GHz and loop probe (with pre-amplifier) as the receiver at these frequencies. In the case of 6GHz both the transmitter as well as the receiver were plate antennas with the same polarisation, but without any pre-amplification. The 1GHz-3GHz experiments were done in order to compare with the previous experiments that were done using the dipole antenna as transmitter. With the 6GHz experiments, the wavelength at this frequency is 5cm, so we could come down to a slot size of 12cm instead of the previous 30.5cm. Because of reduced dimensions of the slots the far-field was brought a little closer. These new slots were made of 3mm thick aluminium covered in black paper.

5.4.1 Double-Slot Experiment at 1GHz

The experiment at 1GHz had the parameters: antenna-to-slot distance = 1m, slot-to-slot distance = 83cm, slot width = 30.5cm, slot-to-detector distance = 3m, power transmitted = 10dBm. The units used are milliwatts. (Fresnel Number for diffraction at slots= 0.001763, Fresnel Number at interference pattern detection = 0.02584)

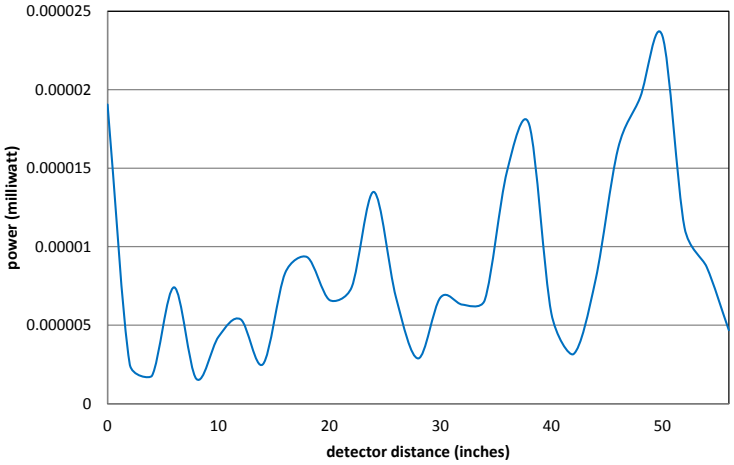

Figure 5.12: Double-slot interference pattern at 1GHz from experiment (transmitter=plate dipole antenna).

Upon comparing this to the previous graphs obtained in Sec. 5.2.2 and Sec. 5.2.3 using the dipole antenna, we observe some consistent features in the interference pattern. Although the double-slot interference pattern has been totally drowned in noise, one can be optimistic that if the errors are consistent and systematic, they can be removed during analysis.

5.4.2 Double-Slot Experiment at 2GHz

The double-slot experiment was performed at 2GHz and the parameters were: antenna-to-slot distance = 1m, slot-to-slot distance = 83cm, slot width = 30.5cm, slot-to-detector distance = 3m, power transmitted = 10dBm. The units used are milliwatts. (Fresnel Number for diffraction at slots= 0.003526, Fresnel Number at interference pattern detection = 0.05168).

The experiment was performed twice, once in the afternoon (trial 1) and once in the evening (trial 2). There is a visible difference in the interference pattern obtained from both cases, which suggests that the environmental disturbances in our experiment, although they might be somewhat consistent during an experiment, are very prone to change depending on the time of the day the experiment is being performed.

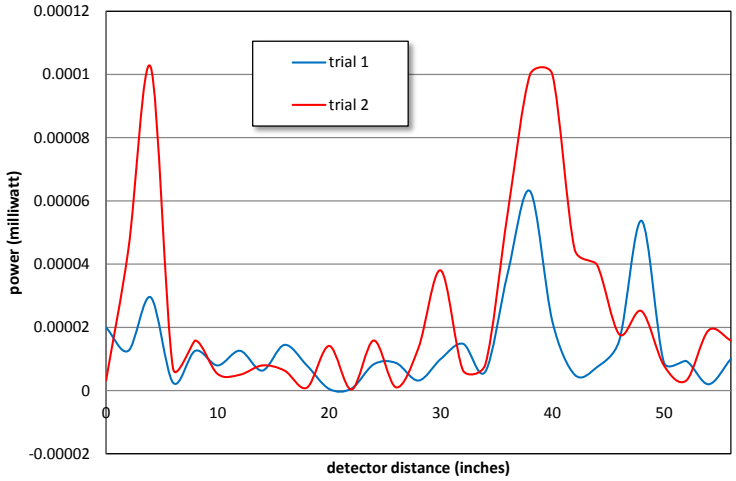

Figure 5.13: Double-slot interference pattern at 2GHz from two sets of experiment on the same day (transmitter=plate dipole antenna).

An important thing to mention would be that the interference pattern in Fig. 5.13 looks pretty similar to those obtained from the 1GHz interference experiments (with both kinds of antennas- dipole antenna and plate antenna) which were performed on the same day as this experiment, but looks rather different from the 2GHz experiment with dipole antenna as the transmitter, which was done on a separate day. Therefore, the environmental disturbances are time-dependent and also differ every day. This makes it important to determine the environmental disturbances explicitly before every single experiment.

5.4.3 Double-Slot Experiment at 3GHz

Using the same set-up we also performed the double-slot experiment at 3GHz with the parameters: antenna-to-slot distance = 1m, slot-to-slot distance = 83cm, slot width = 30.5cm, slot-to-detector distance = 3m, power transmitted = 10dBm. The units used are milliwatts. (Fresnel Number for diffraction at slots= 0.00529, Fresnel Number at interference pattern detection = 0.07752).

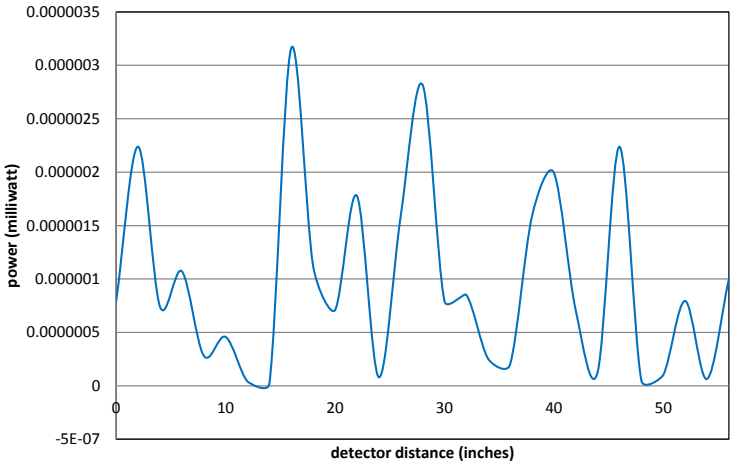

Figure 5.14: Double-slot interference pattern at 3GHz from experiment (transmitter=plate dipole antenna).

Initially it was very difficult to understand why this graph looked so drastically different from the other graphs obtained from experiments performed on the same day (experiments using both kinds of antennas at 1GHz and plate antennas at 2GHz were performed on the same day as this experiment). We soon realised that our pre-amplifier was causing trouble due to some resonance effects at 3GHz, 3GHz being the extreme upper limit of the pre-amplifier.

5.4.4 Double-Slot Experiment at 6GHz

Double-slot experiment at 6GHz was carried out with the detector antenna being a similar plate antenna as the transmitter, with the same polarisation. The parameters were: antenna-to-slot distance = 2m, slot-to-slot distance = 1m, slot width = 12cm, slot-to-detector distance = 6m, power transmitted = 10dBm. The units used are milliwatts. (Fresnel Number for diffraction at slots= 0.00529, Fresnel Number at interference pattern detection = 0.012).

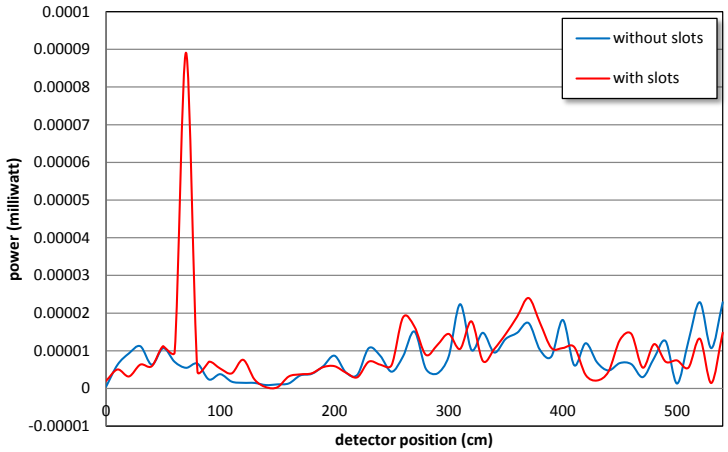

Figure 5.15: Double-slot interference pattern at 6GHz from experiment, overlayed with the antenna radiation pattern at the same distance of detection = 6m(transmitter=plate dipole antenna).

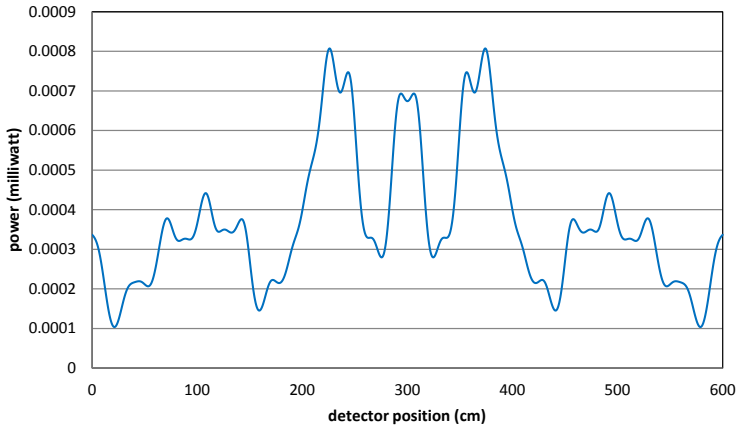

Figure 5.16: Corresponding theoretical plot for double-slot interference pattern at 6GHz from simulation of Huygen's principle in WIPL-D, distance of detection = 6m (parameters are same as those for Fig. 5.15).

The pattern is so messy because of noise that it is impossible to say if the observations are consistent with the theory.

We repeated the experiment with different parameters: antenna-to-slot

distance = 1m, slot-to-slot distance = 1m, slot width = 12cm, slot-to-detector distance = 1m, power transmitted = 10dBm. The units used are milliwatts. (Fresnel Number for diffraction at slots= 0.01058, Fresnel Number at interference pattern detection = 0.072).

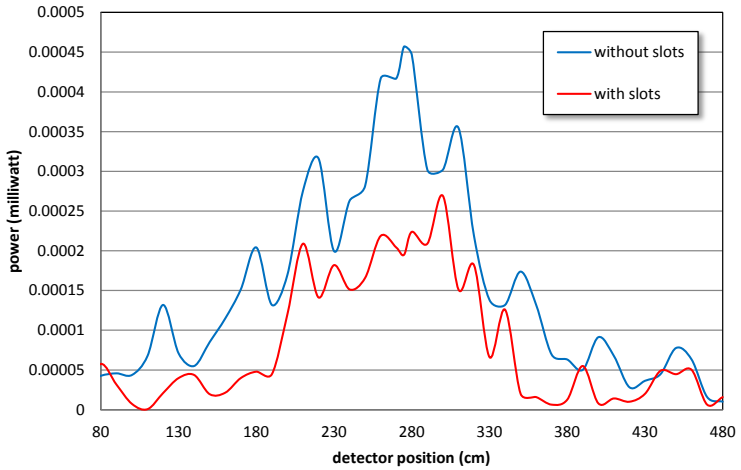

Figure 5.17: Double-slot interference pattern at 6GHz from experiment, overlayed with the antenna radiation pattern at the same distance of detection = 1m(transmitter=plate dipole antenna).

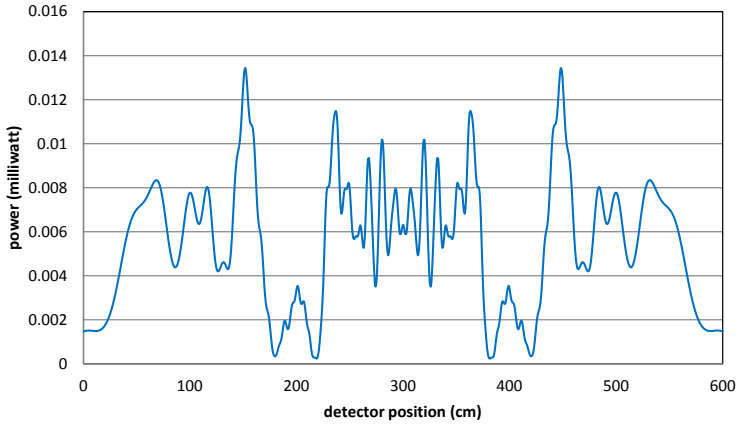

Figure 5.18: Corresponding theoretical plot for double-slot interference pattern at 6GHz from simulation of Huygen's principle in WIPL-D, distance of detection = 1m (parameters are same as those for Fig. 5.17).

We repeated the experiment once again with the parameters: antenna-to-slot distance = 1m, slot-to-slot distance = 1m, slot width = 12cm, slot-to-detector distance = 3m, power transmitted = 10dBm. The units used are milliwatts. (Fresnel Number for diffraction at slots= 0.01058, Fresnel Number at interference pattern detection = 0.024).

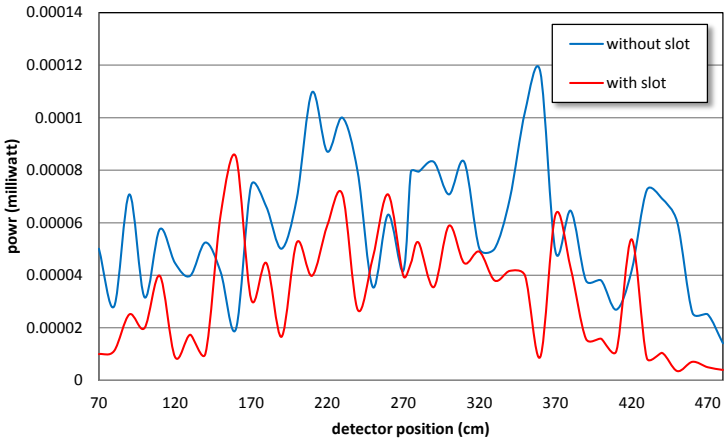

Figure 5.19: Double-slot interference pattern at 6GHz from experiment, overlayed with the antenna radiation pattern at the same distance of detection = 2m(transmitter=plate dipole antenna).

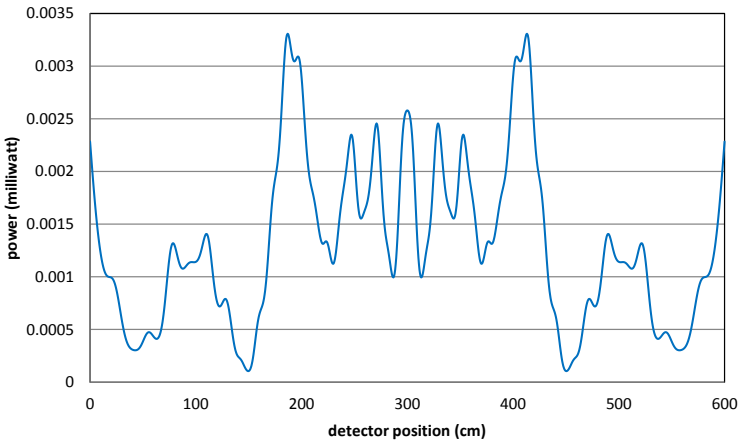

Figure 5.20: Corresponding theoretical plot for double-slot interference pattern at 6GHz from simulation of Huygen's principle in WIPL-D, distance of detection = 2m (parameters are same as those for Fig. 5.19).

As we can see, we were still not able to plot a typical double-slot interference pattern by experiment in the microwave regime. The effect of slots wasn't negligible but the observed interference pattern due to slots still

weren't justified. Especially, the features in the interference pattern did not make sense because they were in the antenna pattern too. The far field had been pushed too far, and also there were a lot of disturbances from the surroundings. A major source of disturbance, as we shall soon see, was the unexpected piece of wood and blue Dow polymer. When we realised this, we repeated the experiment with our new slot stands which were made of thermocol and were hence transparent to 6GHz. This did not seem to solve the problem, however, since we still couldn't get the double-slot interference pattern, although the power being received by the detector was higher in general as compared to our previous experiments.

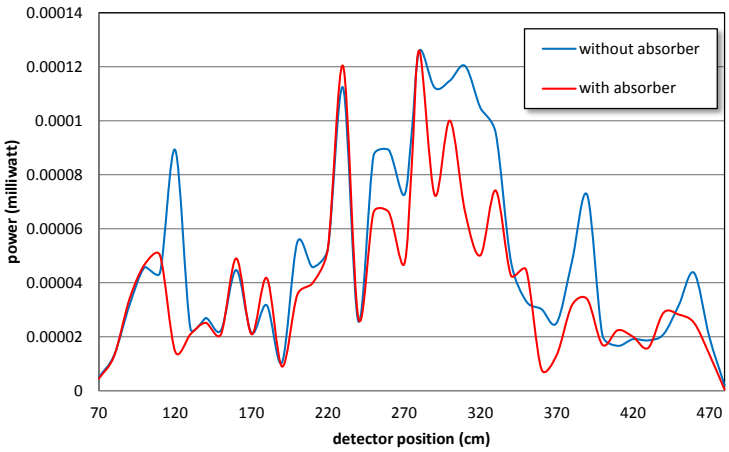

Figure 5.21: Double-slot interference pattern at 6GHz from experiment, with new and more transparent slot-stands. The noise is still too high to see the pattern.

5.5 Determination of microwave transparency of materials at 6GHz

Various materials were tested in order to check their microwave transparency at 6GHz. We plotted the effect of placing a material obstruction between the transmitter and the receiver on the interference pattern due to objects in the surrounding environment that is recorded in the absence of this obstruction. Following are some plots showing the effect of various material obstructions on the detected pattern.

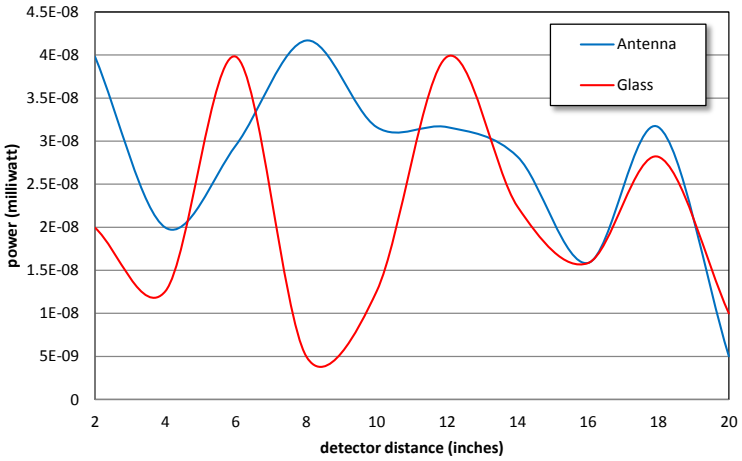

Figure 5.22: Received electromagnetic intensity pattern at the detector in the presence (red) and absence (blue) of a glass barrier.

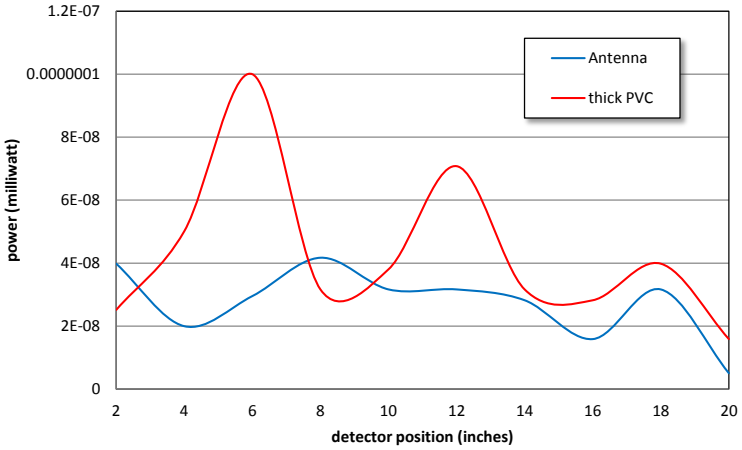

Figure 5.23: Received electromagnetic intensity pattern at the detector in the presence (red) and absence (blue) of a thick PVC barrier.

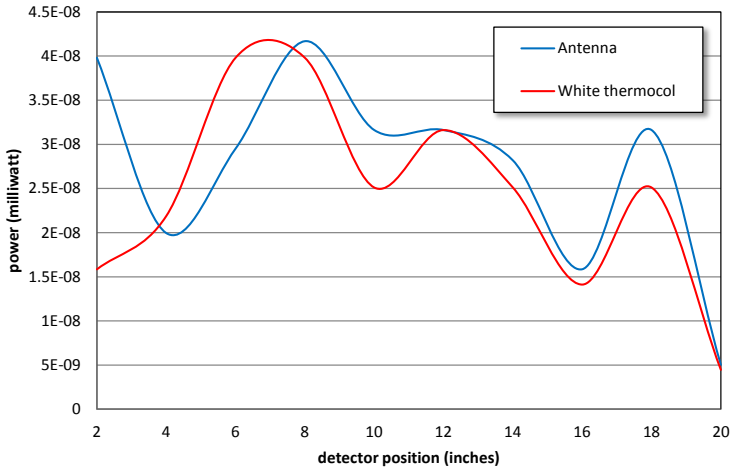

Figure 5.24: Received electromagnetic intensity pattern at the detector in the presence (red) and absence (blue) of a white thermocol barrier.

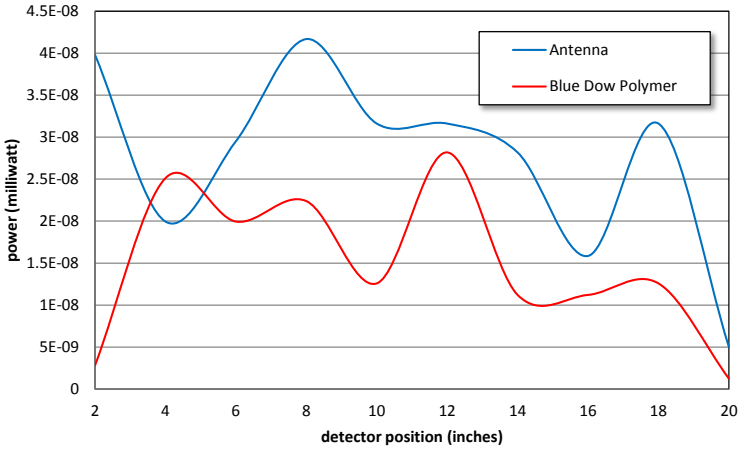

Figure 5.25: Received electromagnetic intensity pattern at the detector in the presence (red) and absence (blue) of a blue Dow polymer barrier.

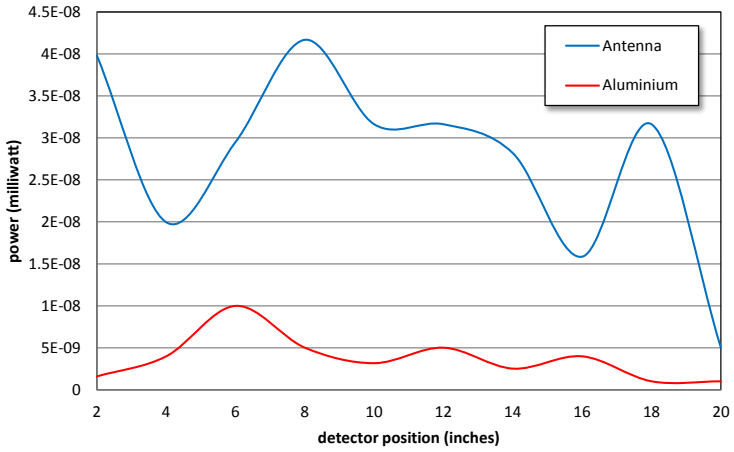

Figure 5.26: Received electromagnetic intensity pattern at the detector in the presence (red) and absence (blue) of a 3mm thick aluminium barrier.

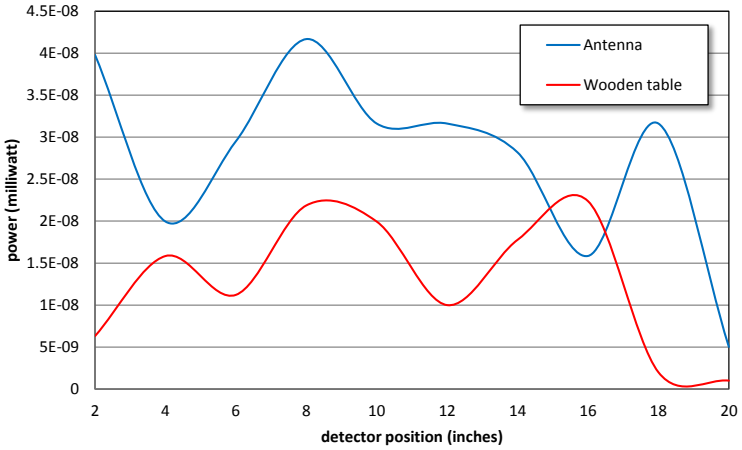

Figure 5.27: Received electromagnetic intensity pattern at the detector in the presence (red) and absence (blue) of a wood (wooden table) barrier.

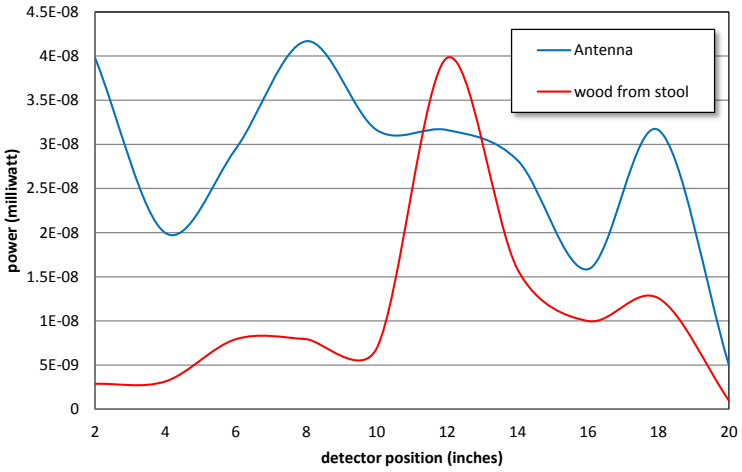

Figure 5.28: Received electromagnetic intensity pattern at the detector in the presence (red) and absence (blue) of a wood (wooden stool) barrier.

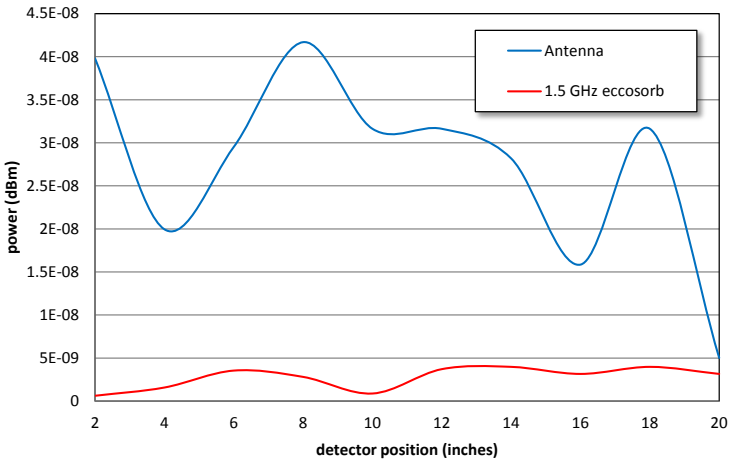

Figure 5.29: Received electromagnetic intensity pattern at the detector in the presence (red) and absence (blue) of an 1.5 GHz Eccosorb sheet barrier.

From the above graphs (Fig. 5.22 - Fig. 5.29), we can't of course quantify the absorbance or transparency of the materials but by looking at them we can qualitatively but very unambiguously conclude that aluminium and Eccosorb sheets are very good blockers of microwaves at 6GHz. Also, white thermocol seems to be the most transparent material.

Although transparent to electromagnetic waves at 6GHz, white thermocol is not a strong material; we cannot use it for making stands that can support aluminium slots. A strong sheet of cardboard could be used to make these stands. In a separate experiment we tested the microwave transparency of cardboard at 6GHz.

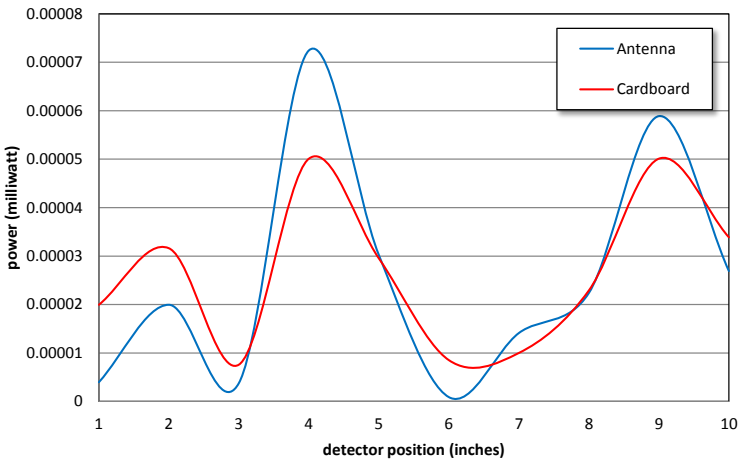

Figure 5.30: Received electromagnetic intensity pattern at the detector in the presence (red) and absence (blue) of a cardboard barrier.

From the Fig. 5.30 we concluded that cardboard was reasonably transparent to electromagnetic waves at 6GHz and could be used for making stands which wouldn't introduce any adverse effect on the interference experiments.

5.6 Differential Measurement of Single Slot and Double Slot interference pattern at 6GHz in the Near Field

Our experiments were not giving us satisfactory results. There could be many reasons for it, one of them being that a lot of radiated power is lost and buried in noise when the distance of detection is large. To check this, we performed an experiment in the near field. Also, we decided to do a differential measurement, the details of this experiment can be found in Sec. 4.2.6 .We measured both single-slot and also double-slot interference patterns. Following are the experimental graphs (red dots) plotted along with

the theoretical curves (blue). They seem to agree decently, in case of the actual interference pattern as well as the differential plots.

5.6.1 Single Slot Interference

Single-slot experiment was performed with the following parameters: antenna-to-slot distance = 60cm, slot width = 12cm, slot-to-detector distance = 60cm, power transmitted = 10dBm. The units used are milliwatts. (Fresnel Number for diffraction at slots= 0.01763, Fresnel Number at interference pattern detection = 0.12).

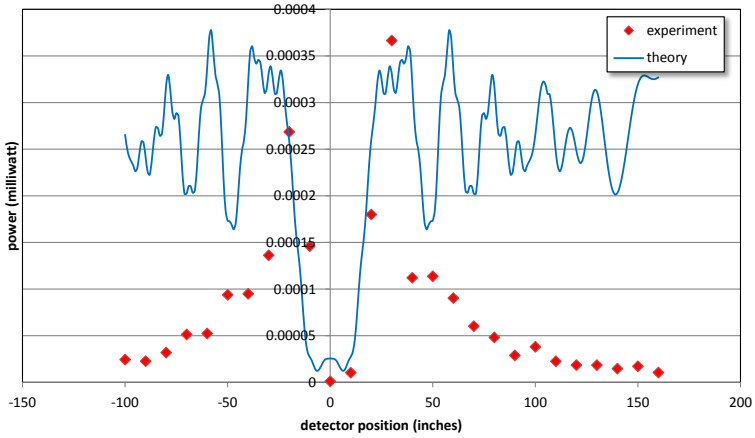

Figure 5.31: Single-slot interference pattern in theory (blue) and experiment (red), detection at 60cm.

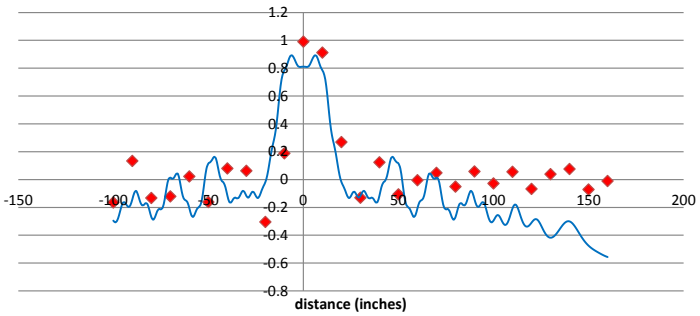

Figure 5.32: Differential plot for single-slot interference pattern in theory (blue) and experiment (red), detection at 60cm. The differential plot shows better agreement with theory.

5.6.2 Single Slot Interference Again

Single-slot experiment was performed with the following parameters: antenna-to-slot distance = 120cm, slot width = 12cm, slot-to-detector distance = 60cm, power transmitted = 10dBm. The units used are milliwatts. (Fresnel Number for diffraction at slots= 0.008816, Fresnel Number at interference pattern detection = 0.12).

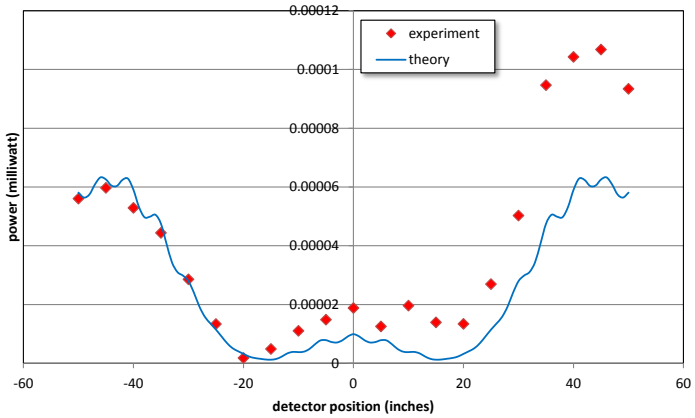

Figure 5.33: Single-slot interference pattern in theory (blue) and experiment (red), detection at 120cm.

5.6.3 Double Slot Interference

Double-slot experiment was performed with the following parameters: antenna-to-slot distance = 120cm, slot-to-slot distance = 30cm, slot width = 12cm, slot-to-detector distance = 60cm, power transmitted = 10dBm. The units used are milliwatts. (Fresnel Number for diffraction at slots= 0.008816, Fresnel Number at interference pattern detection = 0.12).

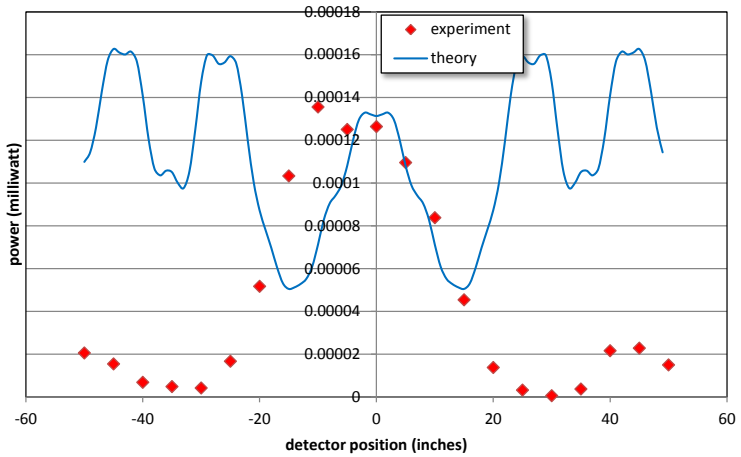

Figure 5.34: Double-slot interference pattern in theory (blue) and experiment (red), detection at 120cm.

We suspect our double-slot pattern is slightly distorted in symmetry because of some defects in the antenna.

5.7 VSWR and Return Loss Measurement at 6GHz

We measured the VSWR and Return Loss for the sleeve dipole antennas we had built. They had a better VSWR value as compared to the plate antennas. At 6GHz this antenna radiates efficiently, with low return loss and a VSWR close to 1.

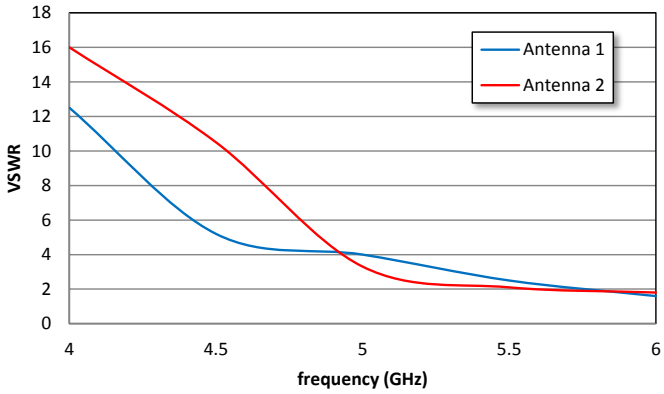

Figure 5.35: Variation of antenna VSWR with frequency for the two sleeve dipole antennas we constructed.

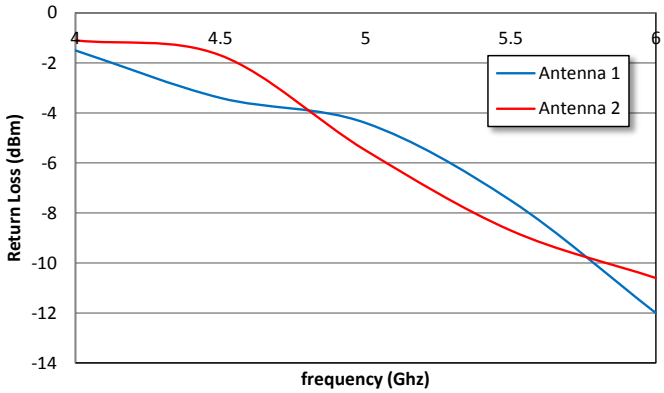

Figure 5.36: Variation of antenna Return Loss with frequency for the two sleeve dipole antennas we constructed.

Chapter 6

Conclusion and Future Directions

Initially, the triple-slit experiments were being performed as a null-test for Born Rule. Over time, we realised a major flaw with the approach, that the triple-slit system cannot represent three disjoint events. There are two possible routes one could take from here: (1) Design other ways to generate three disjoint events, perhaps using interferometers and parametric down-conversion, or (2) Correct for the effects of non-disjointness between the slits, that is, characterise the effect of looped paths on the interference pattern and look for deviations from the resultant pattern. In my project, I have taken the second approach. If the three-way interference term exists and is larger than the effect due to looped paths, we should be able to see its effect in our experiment and hence comment on the validity of Born Rule.

Supposing third-order interference exists, or even higher order interferences exist, the implications would be huge. Born Rule wouldn't be valid any longer, it would only remain a very good approximation. But what is more important is that the generalisation of Quantum Mechanics in this direction could be a starting point of something more fundamental: it might take us one step closer to a Grand Unified Theory.

6.1 Experiments in the Queue

So far, we haven't yet been able to improve the precision of our experiment to the target value. However, we have made a lot of progress in terms of understanding which are the right apparatus for our experiment and developing some important experimental techniques. In order to improve the accuracy of our experiments we plan to take the following steps:

- We may move to an anechoic chamber in order to lower the noise floor

which seems to be drowning the signals. We have already carried out some tests in the anechoic chamber at the Indian Institute of Science, Bangalore. The only drawback here is the limited size of this chamber which will not allow us to go far-field unless we go to very high frequencies.

- The other option to deal with noise is to characterise all the noise sources. We plan to set up our experiment in a large open field and use vector measurement to characterise all reflections. Circulators can be used to minimise reflections off the slots and also the return loss of the antenna.

- We need to minimise the free space loss. We can improve the precision of our measurements by exploiting the phenomenon of beats, by using the phenomenon to convert the radiation to a low-loss frequency in its journey from the slots to the detector and calculating the original interference pattern from the available information.

- We can modify our theory to include near field approximations so that the experiment can also be performed in the near field. This will help solve the problems of loss of radiated power over large experimental dimensions, and also make our approach more universal.

- We plan to purchase more accurate antennas at 6-8GHz, instead of continuing with the home-made antennas which are imperfect.

- If we can acquire a parabolic reflector, we can go far field quickly and easily without having the requirement of very large distances.

6.2 Errors

Error analysis is an important part of any experiment. It is important to have the idea of the noise floor before proceeding to look for a small number like κ, in order to be able to predict whether our experimental design can be fruitful or not. In our experiment, the nature of errors is very different from the ones found in a typical optics experiment. We haven't yet, however, dealt with errors because we are still exploring various experimental set-ups, except for the errors that totally blocked our way to proceed ahead. In that case we have often tried to solve the problem by slightly modifying our experimental design.

6.3 Future Scope

Finding a correction term to the widely believed but not really correct standard theory of slits can have many implications for the future. Some of the possible applications we can see right now include the following:

1. It is the first step towards performing a precision test to verify Sorkin's hypothesis. Since the triple - slit experiment must serve as a null test for Born Rule, the zero of the experiment must have a very low value in order to make sure that any non-zeroness of kappa can be attributed to something which is certainly not arising due to an incorrect theory of slits.

2. Quantum computation experiments using photons require logic gates, which are usually constructed in the laboratory using reflectors and beam-splitters. It is, however, theoretically possible to use simple slits for constructing logic gates for these experiments. Diffracting slits, if arranged in the right manner, can be used as an interferometer. If the slit-interference is fully characterised, a whole new world will open for us, where one can replace interferometers with slit-arrangements, and perhaps even slot-arrangements. One may thus be able to use slits to accomplish quantum computation.

If we successfully prove Sorkin's claim about the existence of third-order interference, the impact on Quantum Computation will be huge.

1. Computational tasks that take two steps could be accomplished in a single step.

2. Ability to efficiently distinguish two states that are exponentially close would allow NP-complete problems to be solved in polynomial space.

References

[1] Sinha, Urbasi, et al. "Ruling out multi-order interference in quantum mechanics." Science 329.5990 (2010): 418-421.

[2] Sawant, Rahul, et al. "Whirling waves in interference experiments." arXiv preprint arXiv:1308.2022 (2013).

[3] Sorkin, Rafael D. "Quantum mechanics as quantum measure theory." Modern Physics Letters A 9.33 (1994): 3119-3127.

[4] Sorkin, Rafael D. "Quantum measure theory and its interpretation." arXiv preprint gr-qc/9507057 (1995).

[5] De Raedt, Hans, Kristel Michielsen, and Karl Hess. "Analysis of multipath interference in three-slit experiments." Physical Review A 85.1 (2012): 012101.

[6] Yee, Kane S. "Numerical solution of initial boundary value problems involving Maxwell's equations." IEEE Trans. Antennas Propag 14.3 (1966): 302-307.

[7] Drozd, Brian, and William T. Joines. "Comparison of coaxial dipole antennas for applications in the near-field and far-field regions." Microwave Journal 47.5 (2004): 160-177.

[8] Sinha, Urbasi, et al. "Testing Born's rule in quantum mechanics with a triple slit experiment." arXiv preprint arXiv:0811.2068 (2008).

[9] SÃűllner, Immo, et al. "Testing born's rule in quantum mechanics for three mutually exclusive events." Foundations of Physics 42.6 (2012): 742-751.

[10] Bonn, Mxx. "On the quantum mechanics of collisions." (1983).

[11] Salgado, Roberto B. "Some identities for the quantum measure and its generalizations." Modern Physics Letters A 17.12 (2002): 711-728.

[12] Jiménez, J. R., and E. Hita. "Babinet's principle in scalar theory of diffraction." Optical review 8.6 (2001): 495-497.

[13] Fedak, William A., and Jeffrey J. Prentis. "The 1925 Born and Jordan paper "On quantum mechanics"." American Journal of Physics 77.2 (2009): 128-139.

[14] Schrödinger, Erwin. "An undulatory theory of the mechanics of atoms and molecules." Physical Review 28.6 (1926): 1049.

[15] Feynman, Richard P., and Albert R. Hibbs. Quantum mechanics and path integrals: Emended edition. Courier Dover Publications, 2012.

[16] Shankar, Ramamurti, Ravi Shankar, and Ramamurti Shankar. Principles of quantum mechanics. Vol. 233. New York: Plenum Press, 1994.

[17] Reck, Michael, et al. "Experimental realization of any discrete unitary operator." Physical Review Letters 73.1 (1994): 58.

[18] Arndt, Markus, et al. "Wave - particle duality of C60 molecules." nature 401.6754 (1999): 680-682.

[19] Scott Aaronson, "Quantum computing, post selection, and probabilistic polynomial-time", Proceedings of the Royal Society, A461, 3473, (2005).

[20] D. Meyer, "Probability sum rules limit the computational benefits of interference", Talk at Canadian Institute for Advanced Research Quantum Information Processing meeting, Alton-Caledon, OT, Canada 25 May 2009.